박사학위논문

Improvement of tropical cyclone intensity predictions using realistic air-sea exchange coefficients and predictors

제주대학교 대학원

해양기상학협동과정

이 우 정

2023년 2월

현실적인 대기-해양 교환계수와 예측인자를 사용한 열대저기압 강도 예측 개선

지도교수 문 일 주

이 우 정

이 논문을 이학 박사학위 논문으로 제출함

2022년 12월

이우정의 이학 박사학위 논문을 인준함

심사위원장 _____㊞

위 원 _____㊞

위 원 _____㊞

위 원 _____㊞

위 원 _____㊞

제주대학교 대학원

2022년 12월

Improvement of tropical cyclone intensity predictions using realistic air-sea exchange coefficients and predictors

Woojeong Lee

(Supervised by professor Il-Ju Moon)

A thesis submitted in partial fulfillment of the requirement the degree of Doctor of Philosophy

2022. 12.

This thesis has been examined and approved.

.....

Thesis director **Sang-Keun, Song**, Prof. of Department of Earth and Marine Sciences in JNU

.....

Il-Ju, Moon, Prof. of Marine Industry and Maritime Police in JNU

.....

Kwang-Il, Kim, Prof. of Marine Industry and Maritime Police in JNU

.....

Nam-Young, Kang, Prof. of Geography Office in KNU

.....

Sok Kuh, Kang, Ph. D. of Korea Institute of Ocean Science and Technology

.....

December, 2022

Interdisciplinary Postgraduate Program in Marine Meteorology

GRADUATE SCHOOL

Contents

Abstract

While tropical cyclone (TC) track forecasts have been improved dramatically for last decades, the accuracy of intensify forecasts over the same time frame has been shown little or no improvement. It is essential to improve TC intensity prediction of statistical and dynamical models because TC forecast of operational centers over the world is closely related with their prediction results. To improve statistical model, a revised predictor called the net energy gain rate (*NGR*) is suggested by considering wind dependent drag coefficient based on the existing maximum potential intensity theory. A series of wind speed dependent *NGR*, known as *NGR-w,* is calculated based on pre-TC averaged ocean temperatures from the surface down to 120 m (at 10-m intervals) to include the TC-induced vertical mixing for 13 years (2004–2016) in the western North Pacific. It turns out that the NGR_{50}-*w* (*NGR*-*w* based on temperature averaged over top 50 m) has the highest correlation with 24-h TC intensity change compared with the commonly used sea surface temperature-based intensification potential (*POT*), depth-averaged temperature-based *POT* (POT_{DAT}), and constant drag coefficient in the *NGR*. To demonstrate the effectiveness of the NGR_{50}-*w*, we designed and conducted experiments for training (2004–2014) and testing (2015–2016). The model with the NGR_{50}-*w* shows greater skill than the model with POT_{DAT} or *POT* by reducing prediction errors by about 16%. To improve dynamic model, we present a new parameterization of air-sea fluxes at extreme wind speeds from 40 m s^{-1} to 75 m s^{-1}, which covers the range of major TCs. Our approach assumes that the TC can reach its maximum potential intensity (MPI) in the absence of influences of external forcing such as vertical wind shear or other environmental constraints. With this method, the ratio of the enthalpy and momentum exchange coefficient (C_k/C_d) under the most intense TCs can be estimated without direct flux measurements. The estimation showed that C_k/C_d increases with wind speed at extreme winds above 40 m s^{-1}. Two types of surface

layer schemes of the Hurricane Weather and Research Forecast (HWRF) were designed based on the wind speed dependency of the C_k/C_d found at high winds: (i) an increase of C_k/C_d based on decreasing C_d (Cd_DC) and (ii) an increase of C_k/C_d based on increasing C_k (Ck_IC). The modified surface layer schemes were compared to the original HWRF scheme (using nearly fixed C_d and C_k at extreme winds; CTRL) through idealized experiments and real-case predictions. The idealized experiments showed that Cd_DC reduced frictional dissipation in the air-sea interface as well as significantly reduced sea surface cooling, making the TC stronger than other sschemes. As a result, Cd_DC reduced the mean absolute error and negative bias by 15.0% (21.0%) and 19.1% (32.0%), respectively, for all lead times of Hurricane Irma in 2017 (Typhoon Mangkhut in 2018) compared to CTRL. This result suggests that new parameterization of C_k/C_d with decreasing C_d at high winds can help improve TC intensity prediction, which currently suffers from underestimating the intensity of the strongest TCs.

Key words: air-sea exchange coefficients, lifetime maximum intensity, maximum potential intensity, numerical modeling, tropical cyclone intensity predictions, Rapid intensification of tropical cyclones

List of Figures

List of Tables

List of Acronyms

C_d	momentum exchange coefficient
C_k	enthalpy exchange coefficient
C_k/C_d	the ratio of the enthalpy and momentum exchange coefficients
DAT	Depth-Averaged Temperature
ENP	eastern North Pacific
HWRF	Hurricane Weather Research and Forecasting Model
JTWC	Joint Typhoon Warning Center
LMI	Lifetime Maximum Intensity
MPI	Maximum Potential Intensity
MPIPOM-TC	Message Passing Interface Princeton Ocean Model-Tropical Cyclone
MWS	Maximum Wind Speed
NA	North Atlantic
NGR	Net energy Gain Rate
NHC	National Hurricane Center
OC_PI	Ocean Coupling Potential Intensity
RI	Rapid Intensification
RMW	Radius of Maximum Winds
SSC	Sea Surface Cooling
SST	Sea Surface Temperature
TC	Tropical Cyclone
WNP	western North Pacific

1. Introduction

Tropical cyclones (TCs) are one of the most dangerous natural hazards, regularly affecting coastal areas socially and economically worldwide. The demand for more accurate forecasts of TC track and intensity is greater than ever because it is evident that very intense TCs are getting more frequent and stronger due to the global warming and climate change (Murakami et al., 2013; Yoshida et al., 2017; Kuntson et al., 2020).

Efforts to improve TC track and intensity forecasts have been tried for past few decades by many scientists. While TC track forecasts have been improved dramatically for last decade, despite years of effort by many researchers and forecasters, the accuracy of intensity forecasts over the same time frame has been shown little or no improvement (Zhang & Tao, 2013; DeMaria et al., 2014). Therefore, improving TC intensity forecasts is still a big challenge for operational TC forecast centers over the world. Improving TC intensity prediction of dynamical, statistical, and statistical-dynamical models is directly related with providing the public with better TC intensity forecasts because they are mainly utilized in intensity guidance.

The representative and widely used method in statistical and statistical-dynamical models is the multiple linear regression. The Statistical Hurricane Intensity Prediction Scheme (SHIPS) based on climatological, persistence, and atmospheric and oceanic predictors affecting to TC intensity using a multiple regression scheme was developed for the Atlantic (DeMaria & Kaplan, 1994) and eastern North Pacific basins (DeMaria & Kaplan, 1999). It has been updated and improved including more smart predictors and realistic data (DeMaria & Kaplan, 1999) and effectiveness of landmasses (DeMaria et al., 2006). In the western North Pacific, the Statistical Typhoon Intensity Prediction Scheme (STIPS) and Decay-SHIPS were developed following methods used by the development of the SHIPS model (Knaff et al., 2005). Kim et al. (2018) investigated that the use of

new predictors ocean-coupling predictors considering TC-induced vertical mixing effects improved the performance of STIPS. Developing a synoptic predictor related to TC intensity or intensity change is essential for improving performance in a statistical-dynamical model.

The Maximum Potential Intensity (MPI), proposed by Kerry Emanuel in the 1980s, is a widely used key predictor to estimate maximum storm intensity given atmospheric and ocean surface conditions. The *MPI* is developed based on the assumption that the TC behaves like a Carnot heat engine. A Carnot engine is a closed system and there are four thermodynamical processes four branches are isothermal expansion, adiabatic expansion, isothermal compression, and adiabatic compression. A Wind-Induced Surface Heat Exchange (WISHE) proposed by Emanuel (1986) is the essential mechanism of TC intensification. It highlights the positive feedback between the ocean and atmosphere in which a stronger heat flux results in a stronger atmospheric circulation, which results in a TC intensification. The *MPI* is reached at the wind speed where the rate of input of available energy into the TC from the sea surface becomes equal to the energy generated by friction acting between the strong wind and sea surface. However, the *MPI* dose not consider the contribution from the subsurface ocean, it may overestimate the maximum intensity of actual TCs. Using a ocean coupling potential intensity (*OC_PI*) including the information on subsurface ocean temperature, Lin et al. (2013) modified the *MPI* used in a statistical-dynamical model and found substantial improvement in performance of using *OC_PI* as a predictor. Balaguru et al. (2015) developed a Dynamic Potential Intensity (DPI) considering ocean conditions and TC information and showed that it explains more variance in TC intensification than *MPI* and *OC_PI*.

Forecasting rapid intensification (RI), defined as 24 hr TC maximum sustained surface wind speed increase greater than 30 knots, has been particularly challenging because of a general lack of understanding of its physical mechanisms. Improving RI forecast skills has been a top priority of the National Hurricane Center (NHC) (Rappaport et al., 2012), because the undergoing RI close to coastal area or

in the middle latitudes may cause serious damage. Kaplan and DeMaria (2003) showed that RI cases were embedded in an environment with specific five large-scale environmental conditions distinct from non RI for Atlantic basin. Using these five predictors, Kaplan et al. (2010) developed SHIPS-RII to estimate the RI probability of RI for Atlantic and eastern North Pacific basins (Kaplan et al., 2010). The SHIPS-RII was enhanced by several new predictors to be more conductive for RI than suggested in Kaplan et al. (2015). TC RI model for WNP was also developed using statistical-dynamical methodology with selected predictors based on past research on RI forecasting (Knaff et al., 2018). More recently, deep learning combined with predictors from dynamical model (Cloud et al., 2019) or statistical-dynamic model (Xu et al., 2021) has been applied to TC intensity prediction.

Improvements in TC intensity prediction using dynamical models have been continuously driven by higher resolution and a better understanding of the dynamics and physics as well as air-sea interactions. A representative dynamic model for TC prediction is the Hurricane Weather Research and Forecast system (HWRF) which was developed at the Environmental Modeling Center of National Centers for Environmental Prediction. The HWRF has been steadily improved with increased spatial resolution, newer data, better modeling techniques, such as data assimilation and TC initialization, after its operation in 2007. One of the main efforts to increase the accuracy of the TC intensity prediction of the HWRF was the improvement of surface layer parameterization schemes calculated from friction velocities and exchange coefficients that enable the calculation of surface heat, moisture and momentum fluxes because the air-sea fluxes of enthalpy and momentum is key to improving intensity prediction (Sroka and Emanuel, 2021).

Many studies focus on the surface fluxes of momentum (C_d) and moist enthalpy (C_k) or their ratio C_k/C_d. Powell et al. (2003) showed that C_d peaked near 40 m s^{-1} in a TC using GPS sonde data. Donelan et al. (2004) showed that the C_d increased with wind speed from 5 to 30 m s^{-1} and did not increase for wind speeds

between 30 and 45 m s^{-1} by using an x-film anemometer to measure the Reynolds stress directly. Soloviev et al. (2014) exhibited that C_d increases with wind speed until approximately 30 m s^{-1}. For winds above 30 m s^{-1}, the C_d nearly levels off and increases again above approximately 60 m s^{-1}. Curcic and Haus (2020) showed that C_d is saturated after the wind speed exceeds 25 m s^{-1} in the laboratory experiments. Haus et al. (2010) showed that C_k is constant for wind speeds between 5 and 35 m s^{-1}. Jeong et al. (2012) estimated C_k using ASIST experiments and showed that sea spray enhanced C_k by at most 38 % when the wind speed is no greater than 13 m s^{-1}. The maximum wind speed of TC strongly depends on the ratio C_k/C_d (Emanuel 1995). Emanuel (1995) suggested that the ratio C_k/C_d lies in the range 0.75 – 1.5 based on the revised theory and numerical modeling results. Bell et al. (2012) showed that the ratio C_k/C_d did not significantly increase for wind speeds greater than 50 m s^{-1} while Solovieve et al. (2014) estimated positive slope of the C_k/C_d ratio ranged from 40 to 60 m s^{-1}. Estimating the ratio C_k/C_d, C_k and C_d in high wind is important for improving TC intensity prediction, but it is challenging to have an accurate value because observations are highly uncertain at high winds. In addition, laboratory estimations of C_d and C_k have also a large degree of uncertainty because of the limitations in realistic representation of the surface factors such as wage age, wave height, spray, and fetch.

To improve TC intensity prediction using a statistical and dynamical methodology, Chapter II describes the new index, net energy gain rate (*NGR*), based on Emanuel's Maximum Potential Intensity theory. The result of statistical model using the *NGR* as a predictor for predicting 24 h intensity changes of western North Pacific TC prediction is also included. Chapter III explores a new parameterization of air-sea exchange coefficients based on the relationship between *MPI* and Lifetime Maximum Intensity (LMI). This includes results from numerical simulations of intense TCs, wherein the sensitivities to each C_k and C_d based on the new parameterization are explored. The concluding chapter summarizes and discusses the key findings of this study.

2. An index to better estimate tropical cyclone intensity change in the western North Pacific

This capter has been published in “Geophysical Research Letter” by the authors (Lee et al., 2019).

2.1. Introduction

While track prediction of tropical cyclones (TCs) has improved steadily over the last three decades (Rappaport et al., 2012), there has been comparatively little advancement in intensity prediction due to the complicated physical mechanisms involved in internal TC dynamics and their interaction with upper-ocean and atmospheric circulation (Elsberry et al., 2013). It is of utmost importance to accurately predict the rapid intensifying and weakening of TCs at the shorter range (within 24 hr) because landfalling TCs can undergo significant and quick intensity changes, which could cause huge economic losses and casualties (Lin et al., 2009). Moreover, landfalling typhoons over the East Asian coast, including China, Japan, Korea, and Taiwan, have shown increased intensity since the late 1970s (Mei and Xie, 2016). Improving rapid intensification forecasts is one of the highest priorities for TC forecasters among many nations and a central focus area of the National Oceanic and Atmospheric Administration’s Hurricane Forecast Improvement Project (Gall et al., 2013).

Numerous attempts have been made to predict the 24-hr intensity change, especially for the rapid intensification cases, based on a statistical-dynamical model (DeMaria et al., 2012; Gao et al., 2016; Kaplan et al., 2010; Rozoff & Kossin, 2011) as well as numerical modeling perspectives (Chen & Gopalakrishnan, 2014; Tallarpragada & Kieu, 2014). According to recent studies, the statistical-dynamical model still shows more skill at all forecast times compared to dynamical models (DeMaria et al., 2014; Kim et al., 2018). Much effort has gone into improving the TC intensity forecast using new predictors (Kaplan et al., 2015), optimizing predictors

(Balaguru et al., 2018; Goni et al., 2009; Rozoff & Kossin 2011), or applying a nonlinear approach (Lin et al., 2017) instead of using the multiple linear regression method. In other words, finding and utilizing a new predictor that accurately represents TC intensity change holds promise for improving forecast performance in statistical-dynamical models.

In exploring the ocean's role in TC intensity changes, it is important to understand the upper ocean thermal structure because of its interaction with TCs (Emanuel et al., 2004; Goni et al., 2009; Kaplan et al., 2010; Lin et al., 2008; Pun et al., 2007; Shay et al., 2000; Wada & Usui, 2007). To estimate the ocean thermal field accounting for the sea surface cooling effect by TC-induced vertical mixing, Price (2009) suggested the depth-averaged temperature (*DAT*),

$$DAT_d = \frac{1}{d}\int_{-d}^{0} T dz, \tag{2.1}$$

where d is the depth of vertical mixing induced by TCs. *DAT* is a more direct and robust metric of the ocean thermal field reflecting interaction between TCs and the ocean than the widely used tropical cyclone heat potential, because the latter may misrepresent oceanic conditions in shallow waters.

MPI is widely used to estimate the maximum surface wind speed given atmospheric and oceanic environment (Emanuel, 1988, 1995). Lin et al. (2013) modified *MPI*, which is determined by the thermodynamic conditions of sea surface temperature (*SST*) and the atmospheric environment for steady state TCs (Emanuel 1988; Holland, 1997), and used *DAT* to form a new *OC_PI* index

$$OC\_PI^2 = \frac{DAT - T_0}{T_0}\frac{C_k}{C_d}(k^* - k), \tag{2.2}$$

where T_o is the TC outflow temperature determined by the atmospheric vertical profile, C_k is the enthalpy exchange coefficient, C_d is the drag coefficient, k^* is the saturation enthalpy of the sea surface, and k is the surface enthalpy in the TC environment. It has been shown that *OC_PI* reduces overestimation of maximum intensity relative to *SST*-based *MPI* (Lin et al., 2013). In recent years, *OC_PI* has been frequently used to predict intensity and rapid intensification (Balaguru et al., 2015; Gao et al., 2016).

The air-sea exchange processes control the evolution of TCs (Emanuel, 2003). The TC intensity depends on the coefficients of the C_d and C_k between the ocean and the atmospheric boundary layer (Emanuel, 1986; Ooyama, 1969). The effects of wind speed-dependent exchange coefficients on TCs have been demonstrated in several previous studies (Braun & Tao, 2000; Bao et al., 2012; Green & Zhang, 2013; Jenkins, 2002; Moon et al., 2007; Nolan et al., 2009a, b), and the parameterizations of C_d were deemed a key determinant of TC intensity simulation. The general consensus is that the C_d increases with wind speed until it reaches approximately 60 kt and does not increase above 70 kt (Bell et al., 2012; Donelan et al., 2004; Jarosz et al., 2007; Powell et al., 2003). However, there are still conflicting results and unresolved issues concerning C_d at very high wind speeds above 120 kt due to limited observations and experiments (Bell et al., 2012; Montgomery et al., 2010; Rotunno & Emanuel, 1987). At extremely high wind speeds above approximately 120 kt, Soloviev et al. (2014) showed that the C_d increases using the unified waveform and two-phase parameterization schemes, whereas Takagaki et al. (2012) showed the value of C_d approaches to constant based on their laboratory measurements. A proper value of C_d at high wind speeds is important to know because the incidence of categories 4 and 5 storms in the northwest Pacific have increased over the last 37 years (Mei & Xie, 2016).

The objective of this study is to improve intensity prediction, especially in a short temporal range of 24 hr. We develop a synoptic predictor for intensity change,

a *NGR*, which is based on *MPI* theory (Emanuel 1988). This predictor is derived from *DAT* and a new parameterization scheme of C_d depending on wind speed. A verification of *NGR* is conducted using a perfect-prognosis based multiple linear regression model for the training and test period. The data and methodology are described in section 2.2. Section 2.3 presents an improvement in *NGR* for TC intensity change. Section 2.4 compares *NGR* with two other comparable new indices suggested by others. Discussion and conclusion are given in section 2.5.

2.2. Data and methods

2.2.1. TC best-track, atmospheric and oceanic data

In this study, TC statistics over the western North Pacific during 2004–2016 are obtained from the best track data archived by the Joint Typhoon Warning Center (JTWC). Statistics for analysis are calculated only for TCs that had a wind speed at or above 34 kt. The *SST* and *DAT* were calculated using the Hybrid Coordinate Ocean Model (HyCOM) Navy Coupled Ocean Data Assimilation (NCODA) nowcast/forecast system data provided by the Naval Research Laboratory. These oceanic variables were averaged within a radius of 200 km from the storm center using prestorm conditions (3 days before). The *DAT* was calculated at various *d* (10–120 m, at 10-m interval; $DAT_{10} - DAT_{120}$) and used to calculate the ocean component of *OC_PI* ($OC\_PI_{10} - OC\_PI_{120}$; hereafter named *OC_PI*s). The *OC_PI*s are calculated based on Emanuel's 'pcmin.m' MATLAB function, which is available online (ftp://texmex.mit.edu/pub/emanuel/TCMAX/pcmin.m). Atmospheric variables were calculated using Global Forecasting System analysis data with 1°×1° spatial and 6-hr temporal resolution provided by the National Centers for Environmental Prediction (NCEP).

2.2.2. The new *NGR*

The energy cycle of a mature TC is one of isothermal expansion, adiabatic expansion, isothermal compression, and adiabatic compression (Bister & Emanuel, 1998). Based on Emanuel's *MPI* theory, the energy generation rate (G) into the TCs from the sea surface for each square meter of sea surface covered by the storm and the surface frictional dissipation rate (D) in the system for each square meter of ocean are given by

$$G = \frac{T_s - T_0}{T_0} C_k \rho V_s (k^* - k), \tag{2.3}$$

$$D = C_d \rho V_s^3, \tag{2.4}$$

where C_k is constant value 1.2×10^{-4}, T_s is *SST* and V_s is the surface wind speed. The *MPI* is reached at the wind speed where the G becomes equal to D. Thus, setting G equal to D and solving for V_s, an expression for the maximum possible sustained surface wind speed of a TC is obtained.

$$MPI^2 = \frac{T_s - T_0}{T_0} \frac{C_k}{C_d} (k^* - k) \tag{2.5}$$

An *NGR* for the western North Pacific basin is developed by incorporating *OC_PI* and wind-dependent drag coefficient based on the *MPI* framework. The *NGR* expresses the realistic response of the sea surface cooling and wave states by TC defined as the difference between *DAT*-based G (G_{DAT}) and wind-dependent C_d-based D (D_w) at the "current intensity" resulting from the given thermodynamic environment.

$$NGR = G_{DAT} - D_w = \frac{DAT - T_o}{T_o} C_k \rho V_s (k_0^* - k) - C_{d(V_s)} \rho V_s^3 \quad (2.6)$$

Larger (smaller) *NGR* implies that the more (less) energy will be used for TC intensification. Note that while *NGR* is the difference between *G* and *D* at the current intensity, when *G* = *D* and therefore *NGR* = 0, the TC reaches a steady state and *MPI* can be derived by solving for *Vs*. The *NGR* was computed and formulated in two ways to conduct a sensitivity test to evaluate the impact of C_d dependence on wind speed for parameterization of the air-sea exchange process. The first one is a default where C_d is set to be a constant (1.33×10^{-3}) in equation (2.6) using the pcmin.m program, hereafter referred to as the "traditional set of *NGR* (*NGR-t*)". The second is derived from equation (2.6) but C_d fitting depending on wind speed is applied instead of the traditionally used constant C_d. For winds below 120 kt, we utilize the unified C_d parameterization scheme interpolated from available field and laboratory data (Soloviev et al., 2014). For winds above 120 kt, C_d is assumed to be constant (2.0×10^{-3}). This will be referred to as the "wind dependency set of *NGR* (*NGR-w*)". The *MPI* is averaged along the track of the storm using the best track data positions at 6-hr intervals excluding current forecast time.

2.3. Results

The intensification potential (*POT*) is defined as the difference between *MPI* and the current intensity. The *POT* is considered the most important predictor in the statistical-dynamical TC intensity prediction models (Chen et al., 2011; DeMaria & Kaplan, 1994, 1999). In particular, *DAT*-based *POT* shows the highest correlation coefficient with intensity change (Kim et al., 2018). We note that, like *POT*, our new predictor *NGR* is also related to the difference between *MPI* and current intensity but the relationship takes a different functional form. Figure 2.1 presents the correlation coefficients between 24-hr TC intensity change and various mixing depths for three groups—*POT*, *NGR-t*, and *NGR-w*—during 2004–2016. Note that the correlation is also carried out for *SST* alone, which is shown at the leftmost margin of the abscissa.

For each individual group, *DAT*-based variables generally exhibit higher correlation coefficients than *SST*-based variables, which are denoted by an open circle in Figure 2.1, revealing the importance of using *DAT*. For example, for *SST* based variables the correlation is 0.48 but it reaches as high as 0.64 at DAT_{90} for *NGR-t* (blue curve). For shallow and moderate *DAT* (≤ 60 m), the *NGR-t* has lower correlations than *POT*. The value of constant C_d (0.0013) used to calculate of *NGR-t* is much lower than the observed C_d in the range from 35 to 63 kt, shown from previous studies, where probability density of observed TC intensity covers 47.7% of the total (not shown). When constant C_d, is used the *D* for *NGR-t* is underestimated, which results in lower correlation with 24-hr TC intensity change than *POT* for *DAT* ≤ 60 m. The *DAT*-based *POT* (black curve) correlates significantly with the intensity change at the 1% test level as reported in a previous study (Kim et al., 2018). Note that an even higher correlation coefficient (0.69) is found between the TC intensity change and *DAT*-based *NGR-w* (red curve). This implies that the dependence of the wind speed on C_d in many studies is important because C_d plays an important role

in contributing to the energy budget for TC intensity. Because *NGR-w* using a wind speed dependent C_d represents the TC energy budget more realistically than *NGR-t* using a traditional constant C_d, this new predictor is likely to exhibit the highest correlation to 24-hr TC intensity change.

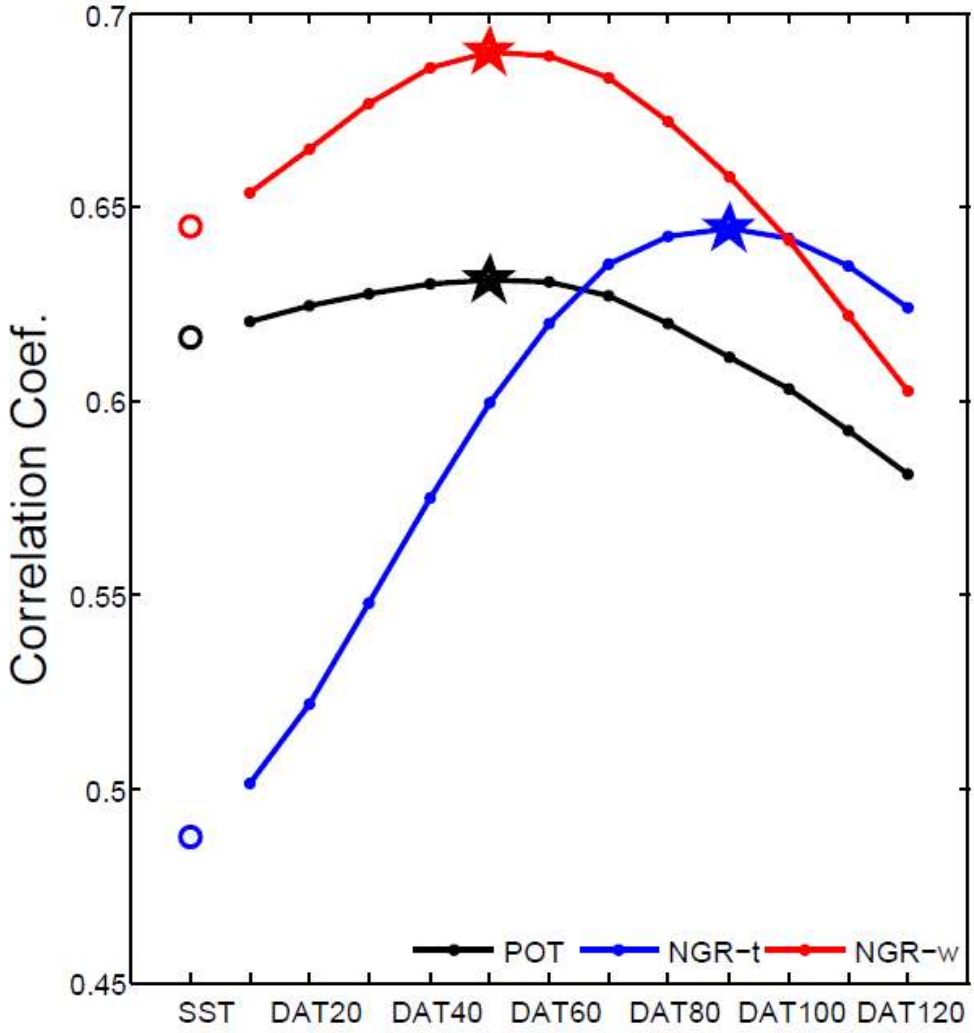

Figure 2.1. The comparison of the correlation coefficients between a series of *POT*, *NGR-t,* and *NGR-w* from *SST* to DAT_{120} by computed ocean temperature averaged over surface to 120-m depth (at 10-m interval) and the 24-hr changes in TC intensity during 2004–2016. Pentagrams represent the location of maximum value for each group (*POT*=the intensification potential; *NGR-t*=net energy gain rate using constant drag coefficient; *NGR-w*=same as *NGR-t* but for changing drag coefficient).

It is somewhat surprising that the correlations between *NGR*-*w* and intensity change drop dramatically for *DAT* ≥ 80. It is well known that the strength of maximum wind speed is the dominant factor in TC-induced vertical mixing and the typical vertical mixing depth for a major TC (category 3 to 5) is about 100 m (Price, 2009). The deep mixing depth (≥ 80 m) based on *DAT* is suited for strong TCs, but can cause underestimation of *G* in equation (2.3) for relatively weak TCs. Therefore, the correlation coefficient of deep *DAT* based-*NGR* is lower because the *DAT* used is too deep (or too cold) for weak TCs and the frequency of strong TC events is very low.

Table 2.1. Experimental designs for investigating the effect of using the NGR_{50}-*w* on 24-hr TC intensity change. The correlation coefficients between the predictors and 24-hr TC intensity change during 2004–2016 are indicated in parentheses. The numbers in the subscript of *POT* and *NGR* refer to the depth of the ocean (in meters). The *PER* and *SHRD* indicate previous 12-hr intensity change and 850- to 200-hPa vertical wind shear. Mean absolute error (MAE) and R^2 of 24-hr TC intensity changes for four experiments are also compared during the training period (2004–2014) and test period (2015–2016).

Experiment	Predictor 1	Predictor 2	Predictor 3	Training period (2004–2014)		Test period (2015–2016)	
				MAE (kt)	R^2	MAE (kt)	R^2
EXP1	*POT* (0.62)	*PER* (0.39)	*SHRD* (-0.36)	12.04	0.51	13.18	0.38
EXP2	POT_{50} (0.63)			12.02	0.51	13.07	0.40
EXP3	NGR_{90}-*t* *(0.64)*			12.26	0.48	12.40	0.43
EXP4	NGR_{50}-*w* (0.69)			11.42	0.55	11.33	0.51

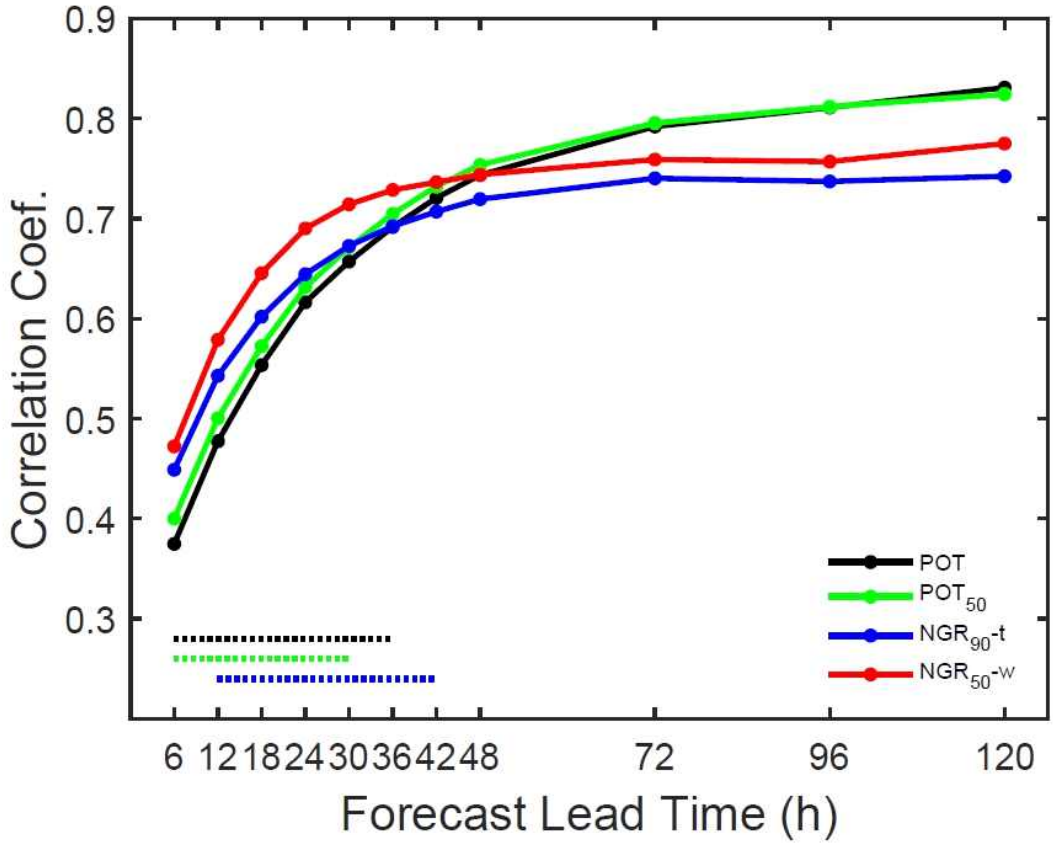

Figure 2.2. The comparison of the correlation coefficients between *POT*, POT_{50}, NGR_{90}-*t,* and NGR_{50}-*w* and TC intensity change at each forecast lead time during 2004–2016. For each forecast time the *MPI* is averaged along the track of the storm using the best track data positions at 6-h intervals excluding current forecast time when each predictor is calculated. The dashed lines indicate the forecast lead time ranges whichwhere correlation coefficients of NGR_{50}-*w* isare significantly significant at the 95 % confidence level based on Fisher's z test compared with other predictors. (5% test level) higher than other factors.

The correlation coefficient of *DAT*-based *POT* for the longer lead times after 42-hr tends to be higher than *NGR*-*w* (Figure 2.2). This is due to the use of the TC current intensity when the *G* and *D* are calculated in equation (2.6). Consequently, the TC intensity uncertainty increases with increasing forecast lead time. According to the Fisher's z test (Wilks, 2011), the difference in the correlation coefficient between *NGR*-*w* and other predictors is significantly different within 42-hr forecast lead times as denoted by the dashed lines in Figure 2.2 at the 5% test level (e.g., the p-value

is smaller than 0.05). Note that *DAT*-based *NGR-w* attains the maximum correlation coefficient with 24-hr TC intensity changes at 50 m (Figure 2.1). In Figure 2.3, we compare the spatial distribution of the composite of 24-hr observed TC intensity change, NGR_{50}-*w*, *POT*, and *POT* at DAT_{50} (POT_{50}) for the period 2004–2016. The areas of observed positive TC intensity changes span the main TC development region (5°–20°N, 110°–160°E) in the warm pool of the Philippine Sea and the South China Sea before making landfall or undergoing extratropical transition (Figure 2.3a). The regions of negative TC intensity changes are found from the Yellow Sea extending northeastward through the Kuroshio extension region. The *POT* and POT_{50} have patterns similar to the observations but show TC intensity changes that are too strong throughout the main TC development region and too weak or rare at higher latitudes (Figures 2.3c and 2.3d). On the other hand, the NGR_{50}-*w* has a distribution closest to the observations in both positive and negative TC intensity change regions (Figure 2.3b). The pattern correlations between the observed 24-hr TC intensity change and the corresponding *POT*, POT_{50}, and NGR_{50}-*w* are computed over a 1° latitude-longitude box centered at each grid point for the period of 2004–2016. The correlations are 0.66, 0.68, and 0.77 for the aforementioned three predictors, respectively, and the correlation between NGR_{50}-*w* and intensity change is statistically significant at the 1% level (Chu & Zhao, 2007) when Quenouille's (1952) method is used to account for the reduction in the effective number of degrees of freedom due to persistence. This result lends support that the NGR_{50}-*w*, which has the highest pattern correlation coefficient and captures most of the observations for a 24-hr TC intensity change. To compare the prediction skill of the main predictors (*POT*, POT_{50}, NGR_{90}-*t* and NGR_{50}-*w*), perfect prognosis-based multiple linear regression models are developed for 24-hr intensity change based on a combination of each of the aforementioned main predictors, together with previous 12-hr intensity change (*PER*) and 850- to 200-hPa vertical wind shear (*SHRD*). The last two predictors are widely used for intensity prediction and are always included as two additional predictors (Gao et al., 2016; Knaff et al., 2005; Kaplan et al., 2015). As listed in

Table 2.1, four sets of experiments are designed: (1) a run with the use of *POT* (hereafter referred to as the EXP1); (2) a run with the use of DAT_{50}-based *POT* (POT_{50}) (hereafter referred to as the EXP2); (3) a run with the use of DAT_{90} based *NGR-t* (NGR_{90}-*t*) (hereafter referred to as the EXP3); and (4) an experiment using the NGR_{50}-*w* (hereafter referred to as the EXP4). The four experiments are conducted to predict the 24-hr TC intensity change over the western North Pacific during 2004–2016. The *SHRD* is averaged within a 200-km radius after vortex removal.

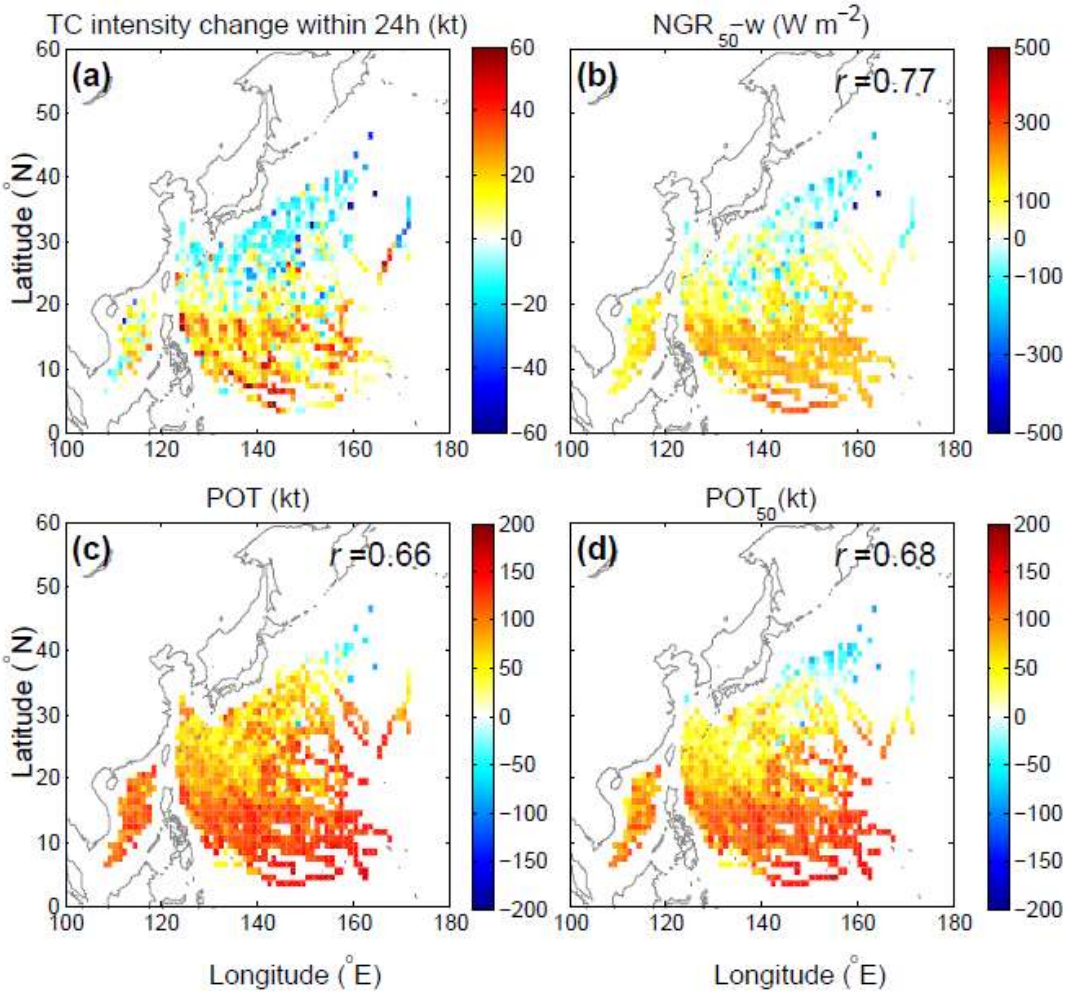

Figure 2.3. Composite (a) 6-hourly observed 24-h TC intensity change (kt), (b) NGR_{50}-*w* (Wm^{-2}), (c) *POT* (kt), and (d) POT_{50} (kt) in the 1°x 1° grid boxes during the period 2004–2016. The numbers in the top-right corner of (b)–(d) panel denote the correlation coefficient with (a).

The performance of four models in terms of mean absolute error (MAE) and R^2 (coefficient of determination) is estimated from the training (2004–2014) and test (2015–2016) periods. For the training period, MAE and R^2 were compared among the four models. Results show that EXP1 (using *POT*) is comparable to EXP2 (using POT_{50}) and EXP3 (using NGR_{90}-*t*), while EXP4 (using NGR_{50}-*w*) shows the best performance (Table 2.1). EXP4 explains the highest R^2 (55%) and has the lowest error (11.42 kt). For the independent period, the NGR_{50}-*w* is, again, the best predictor with the lowest error and highest R^2 among four experiments (Table 2.1). Relative to EXP1, the 24-hr intensity change error decreases by up to 16% when the predictor NGR_{50}-*w* is used. These improvements in the EXP4 for the training (test) period are statistically significant at the 5% (1%) level. Because the NGR_{50}-*w* more realistically characterizes the interaction between TCs and the ocean using C_d depending on wind speed compared with NGR_{90}-t that uses a constant C_d, it serves as an effective predictor in improving prediction of TC intensity change at the shorter lead times (within 24 hr).

A comparison of the correlation coefficients between 24-hr TC intensity change and each of three groups (*POT*, *NGR-t*, and *NGR-w*) are also examined by classifying TCs into seven intensity categories according to initial maximum wind speed: tropical storm (34–47 kt); severe tropical storm (48–63 kt); category 1 (64–82 kt); category 2 (83–95 kt); category 3 (96–112 kt); category 4 (113–136 kt); and category 5 (above 137 kt). Figure 2.4a shows the maximum correlation coefficients from *SST* to DAT_{120} for 24-hr TC intensity changes for three groups. Figure 2.4b displays the mixing depth with the highest correlations for the seven TC categories and all three groups. When storms are in the weakest stage (tropical storm), the highest correlations are almost identical for all three groups and occur at a very shallow mixing depth (~10 m) as shown in Figure 2.4b. Intense TCs tend to have higher correlations with a deeper *DAT* for all groups and intensity categories. It also appears that the average mixing depth for *NGR-w* is ~50 m (Figure 2.4b). As expected, the *NGR-w* exhibits a higher correlation with 24-hr TC intensity change

than *POT* for intensities below category 3 (Figure 2.4a), while *NGR-w* does not perform as well for the intensities above category 4. In fact, the *NGR-w* has the lowest correlation coefficient among these three groups, especially for the intensities above category 5. This implies that constant C_d (2.0×10^{-3}) at extreme winds may not be optimal and one may parameterize C_d with an increasing or a decreasing value or a constant but different value. The behavior of the air-sea exchange coefficient is controversial and still unclear at extreme wind speeds. We will return to this point later.

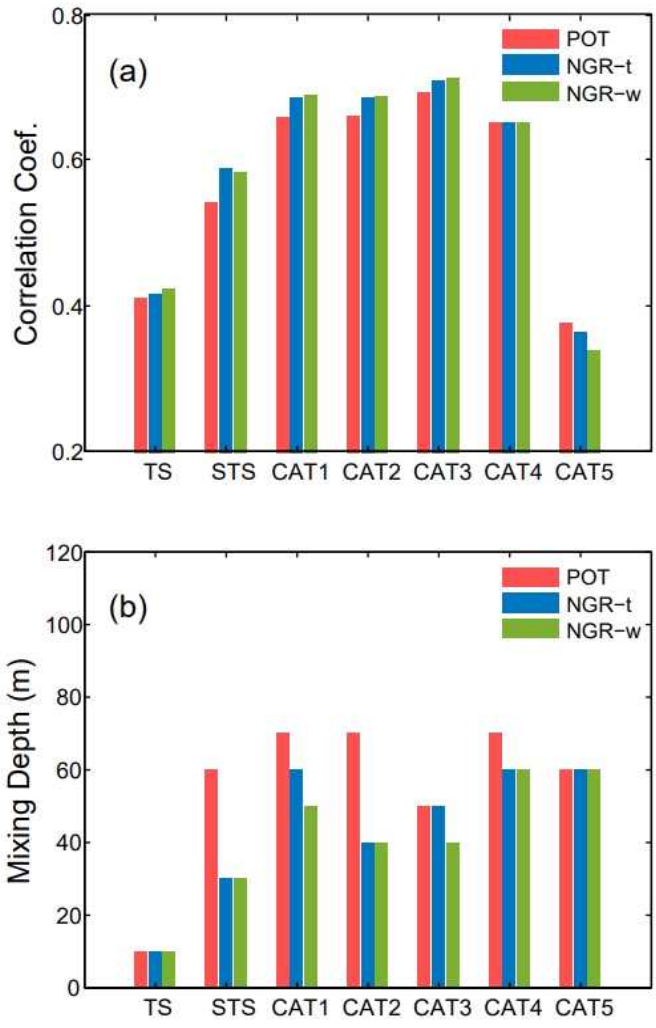

Figure 2.4. A comparison of the (a) maximum correlation coefficients from *SST* to DAT_{120} between 24-hr TC intensity change for three groups and (b) the mixing depth with the highest correlations by classifying TCs into seven intensity categories.

2.4. A comparison with predictors from other recent studies

This study also examined the effect of the use of TC-induced mixing depth varying with an individual TC state (T_{dy}). This is motivated by recent studies (Balaguru et al., 2015, 2018) that suggest using T_{dy} yields a better prediction of TC intensification based on the NHC's Statistical Hurricane Intensity Prediction Scheme. Following Balaguru et al. (2015) we calculate T_{dy} from the JTWC archive and HyCOM data for the same period and use the wind dependent C_d as applied to *NGR-w* as described in section 2.2 (NGR_T_{dy}). Our results show that NGR_T_{dy} has a lower correlation (r = 0.64) with 24-hr TC intensity than NGR_{50}-w (r = 0.69), which is contrary to our expectations. However, the difference in correlations between Balaguru et al. (2015, 2018) and our study is not statistically significant.

A possible reason for this result could be the TC-wave-ocean coupling effect on momentum flux. Fan et al. (2009, 2010) showed that momentum flux is significantly reduced because of the strong dependence on the wave-induced processes near the ocean subsurface in a fully coupled wind-wave-ocean model. This reduction can be as large as 25% depending on the choice of the C_d parameterization. The parameterization of TC-induced mixing depth is therefore recommended to include the effect of wave-current interaction. Further studies are needed to find out more realistic drag coefficients when waves are incorporated in the parameterization scheme.

As mentioned previously, the behavior of C_d under very high wind speed conditions is uncertain although the *NGR-w* used here is wind dependent up to 120 kt. It might be possible for C_d to increase (Soloviev et al., 2014) or not change significantly at extreme wind speeds (Bell et al., 2012). It would be interesting to compare the results of *NGR-w* to an *NGR* using an increasing C_d above 120 kt (*NGR-i*). A series of *NGR-i* is calculated (Soloviev et al., 2014) and we find that *NGR-i* also has a high correlation with 24-hr TC intensity change for all *DAT*. The

maximum correlation coefficient of *NGR-i* is 0.68 at DAT_{50}, which is slightly lower than the NGR_{50}-*w* (r=0.69). Therefore, in cases where C_d at very high wind speed is not known, a constant C_d may be used.

2.5. Discussion and conclusion

A statistical-dynamical technique for TC intensity prediction combining statistical methodology with environmental predictors derived from numerical weather prediction system has been widely used over the last 25 years (DeMaria et al., 2005; DeMaria & Kaplan, 1994; DeMaria & Kaplan, 1999). The development of a new predictor, which has a high correlation with TC intensity, is directly connected to the improvement in prediction skill for a statistical-dynamical model.

DAT-based *POT* shows higher correlation with 24-hr intensity change than *SST*-based *POT*. However, for all the *DAT* (10–120 m) including *SST*, *NGR*-*w* has higher correlations than *DAT*-based *POT* (Figure 2.1) and improved 24-hr TC intensity prediction using NGR_{50}-*w* is achieved during both the training and independent periods (Table 2.1). The addition of a wind dependent C_d to the dissipation term in *NGR*-*w* thus led to better prediction results for 24-hr intensity change. The findings in this study indicate that the best performance in predicting 24-hr TC intensity change was by the model at depth of 50 m (DAT_{50}). This is somewhat different from the results of Price (2009) and Lin et al. (2013), who suggested that the best results for the ocean thermal field representing TC-ocean interaction are obtained from DAT_{100} and DAT_{80}, respectively. This difference may be attributed to the fact that all TC cases are used in this study while the two previous studies only focused on stronger TCs.

To improve TC intensity change or rapid intensity change forecasts, this study suggests that *POT* predictors may be replaced by NGR_{50}-*w* because the latter more realistically represents the ocean contribution to 24-hr TC intensity change. In addition, the NGR_{50}-*w* can be used to analyze the 24-hr TC intensity changes in the currently best performing intensity prediction models such as the Statistical Hurricane Intensity Prediction Scheme and Statistical-dynamical Typhoon Intensity Prediction Scheme, because both models show little improvement at the shorter ranges (24–48

h) (DeMaria et al., 2014).

Many studies have shown that TC intensity change is closely related to *DAT* and the parameterization of the air-sea exchange processes. We propose *NGR*, a new variant of an intensity change predictor related to Emanuel's MPI that uses the *DAT*, which includes information from TC-induced vertical mixing, and C_d dependent on wind speed (instead of a traditional constant C_d). We show that the new index, NGR_{50}-*w*, improves the hindcasts of 24-hr TC intensity change and anticipate that this new index will contribute to improvements in real-time TC intensity forecasts, not only for the western North Pacific but also for other basins.

The NGR_{50}-*w* showed an overall positive bias (Figure 2.5) for a steady-state condition. This implies that in addition to frictional dissipation, other environmental factors such as vertical wind shear might be considered with TC intensity changes in real time forecasts. Lin et al. (2013) reported that *OC_PI* is overestimated by about 10–20% because the atmospheric portion of the MPI equation is calculated under the assumption that the atmospheric profile does not have sufficient time to quickly adjust to the *DAT*. In this study, the *G* is also calculated in the same manner, which results in positive bias of NGR_{50}-*w* for a steady state. In addition, it should be noted that the correlation of NGR_{50}-*w* with intensity change is higher than the other predictors at shorter ranges (within 42 hr). Indeed, this result was statistically significant based on the Fisher's z test, at the 5% test level from 6 to 36, 6 to 30 and 12 to 42 hr compared with the correlation of *POT*, POT_{50}, NGR_{90}-*t*, respectively, while after 48 hr the correlation coefficient does not reach 95% significance (Table 2.2). This is because the value of intensity dependent *NGR* is calculated by the TC current intensity. Therefore, the TC intensity uncertainty increases with increasing forecast lead time and inconsistency between initial wind strength and TC intensities at the forecast lead times also increases.

We showed that the *NGR* index better estimates TC intensity change in the western North Pacific. Future work will apply the *NGR* index to other TC basins and verify that DAT_{50} shows the best performance in predicting 24-hr TC intensity

change in this study with other years and other basins.

Table 2.2. The *p*-values of the difference in correlation coefficient between NGR_{50}-*w* and the other predictors for each forecast lead time using Fisher's z test. Negative z signs are in bold.

	Forecast lead time (h)										
	6	12	18	24	30	36	42	48	72	96	120
POT	0.0000	0.0000	0.0000	0.0000	0.0000	0.0037	0.2213	0.9681	**0.0096**	**0.0003**	**0.0008**
POT_{50}	0.0001	0.0000	0.0000	0.0000	0.0009	0.0561	0.7414	**0.4295**	**0.0040**	**0.0002**	**0.0035**
NGR_{90}-*t*	0.1902	0.0226	0.0025	0.0006	0.0012	0.0045	0.0214	0.0561	0.1835	0.2420	0.1010

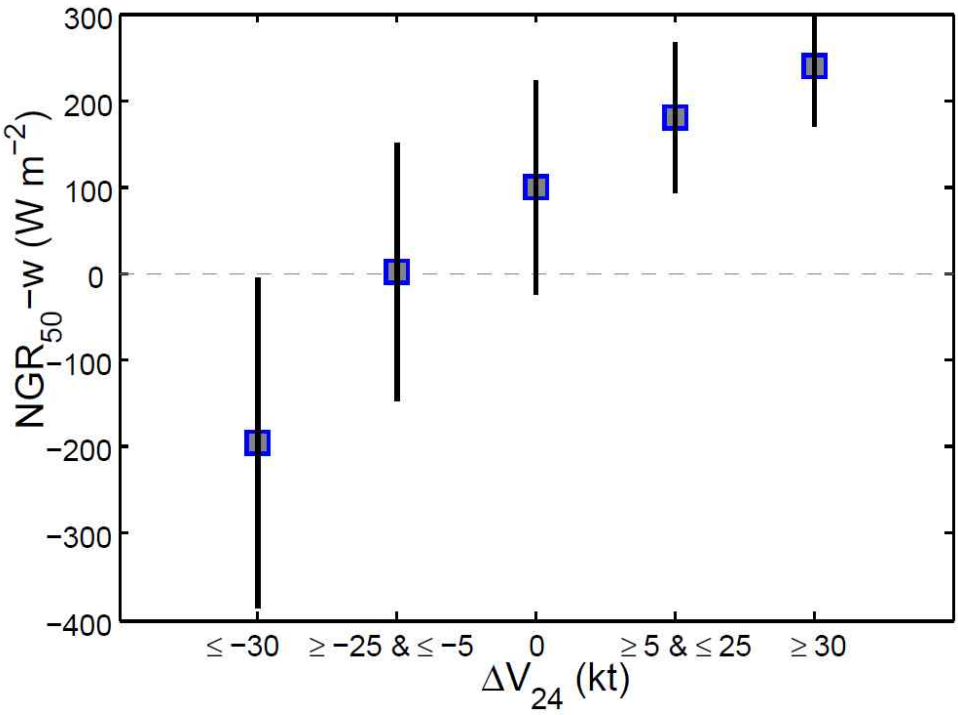

Figure 2.5. Box plot of mean and one standard deviation values of the NGR_{50}-*w* for five 24-hr TC intensity change categories during 2004–2016: rapidly intensifying (≥30 kt); intensifying (≥5 kt & ≤25 kt); steady-state (0); weakening (≥-25 kt & ≤-5 kt); and rapidly weakening (≤-30 kt).

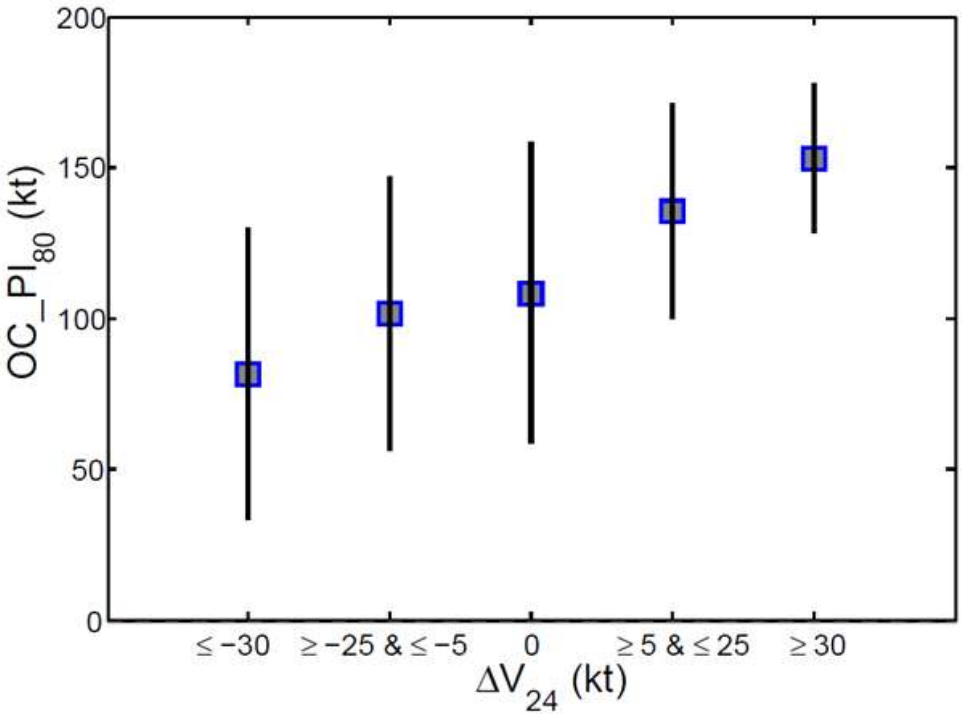

Figure 2.6. Same as Figure 2.5 but for the *OC_PI*$_{80}$.

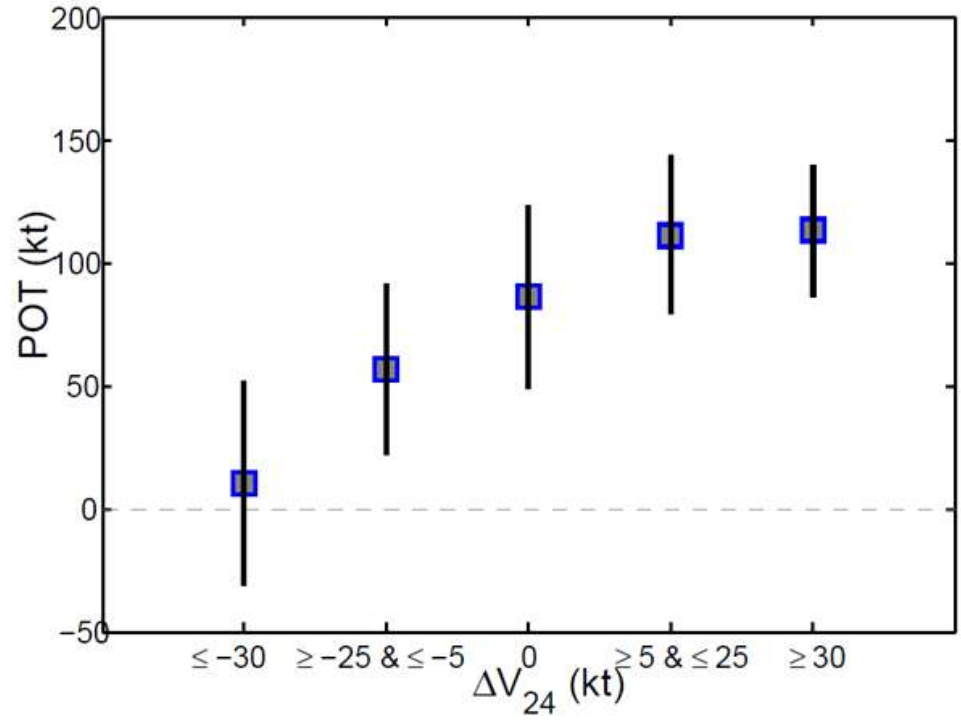

Figure 2.7. Same as Figure 2.5 but for the *POT*.

3. New parameterization of air-sea exchange coefficients and its impact on intensity prediction under major tropical cyclones

This chaper has been published in “Frontiers in Marine Science” by the authors (Lee et al., 2022)

3.1. Introduction

Prediction of the tracks of TCs has significantly improved over the last decades, but there has been less progress in intensity prediction despite the considerable advancement in technologies for TC-related physics, computational power, numerical modeling, and observations during the same period (DeMaria et al., 2014; Soloviev et al., 2014). TC intensity prediction is challenging because the various environmental effects, inner core dynamics, and underlying surface forcings involved in the intensity change are not entirely understood (Elsberry et al., 2013). In particular, the unresolved physics of the momentum and enthalpy transfer between the atmosphere and the ocean at extreme wind speeds are crucial factors that hamper accurate TC intensity prediction (Moon et al., 2004; Moon et al., 2007).

Figure 3.1 shows the bias of the HWRF in predicting the 10 m maximum wind speed (MWS) for 2016-2020 in the North Atlantic (NA), the eastern North Pacific (ENP) and the WNP TCs, on the basis of 82,821 predictions. The HWRF is an atmosphere-ocean coupled model customized for hurricane or tropical storm application (Biswas et al., 2018); it is a real-time TC forecasting system operational at the National Centers for Environmental Prediction (NCEP) since the 2007 TC season. Overall, a negative bias (underestimation) is evident above 40 m s^{-1}, significantly increasing with MWS (Figure 3.1). It reaches −20 m s^{-1} for intense TCs with an MWS above 80 m s^{-1}. This large bias may be partly attributed the insufficient horizontal grid resolution of the model. Another possible reason is the

inadequate representation of some physical processes, including the air-sea momentum and enthalpy exchanges at high wind speeds.

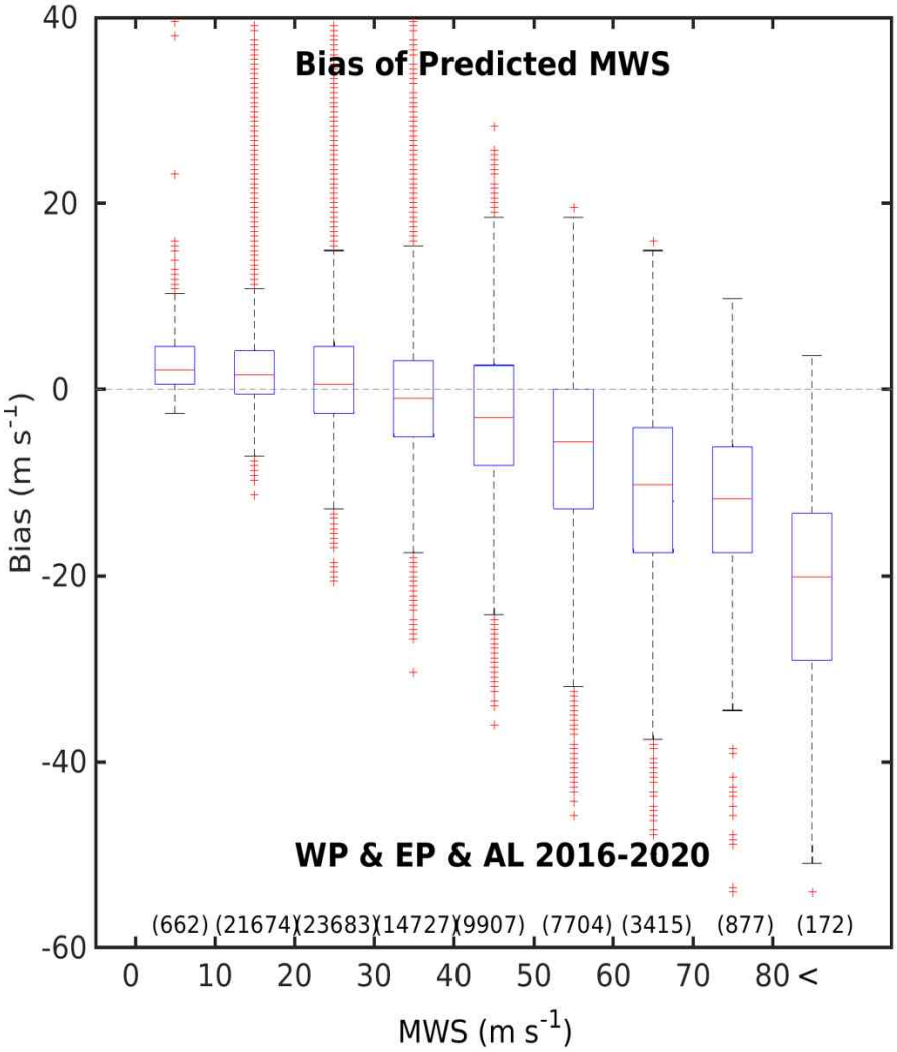

Figure 3.1. Evaluation results of operational HWRF intensity predictions for 82,821 TC cases in 2016-2020 NA, ENP and WNP. The values represent the bias of the predicted MWS against that of the measured MWS. The candle bars indicate the medians (red horizontal bars) and their 95% confidence intervals (dashed bars) for biases within each 10 m s^{-1} interval of the MWS. The numbers in parentheses above the x axis denote the assigned TC case number.

TC intensity depends strongly on the coefficients of the C_d and C_k between the ocean and the atmospheric boundary layer (Ooyama, 1969; Rosenthal, 1971; Emanuel, 1986). In particular, the theoretical MWS of a TC depends on the ratio of the enthalpy coefficient to the momentum exchange coefficient—$(C_k/C_d)^{1/2}$—in the high–wind speed core of the storm (Emanuel, 1986). Estimating the most accureate C_k/C_d and its behavior at high wind speeds is essential for accurate TC intensity prediction (Green and Zhang, 2013; Soloviev et al., 2014).

The perceived importance of the dependence of the TC intensity on the C_k/C_d has led to considerable effort to measure the exchange coefficients at hurricane-strength wind speeds (DeCosmo et al., 1996; Black et al., 2007; French et al., 2007; Zhang et al., 2008; Haus et al., 2010; Bell et al., 2012; Hsu et al., 2019; Curcic and Haus 2020; Richter et al., 2021). However, these observations deliver less accuracy at high winds. For exchange coefficient estimates based on the mean profile data obtained from dropsondes in TCs, the accuracies are known to be 50% and 200% for C_d and C_k, respectively (Richter et al., 2016). Likewise, laboratory estimations of C_d and C_k have limitations because conditions of field observations such as wave age, wavelength, spray, and fetch cannot be considered realistically. These limitations make the determination of air-sea exchanges at extreme wind speeds and their wind dependency difficult (Richter et al., 2016).

In this study, we propose an alternative method in which C_k/C_d at very high wind speeds is indirectly estimated by matching the observed LMI of a TC with the theoretical MPI. This method is based on the assumption that the LMI can reach the MPI if there are no negative influences on the maximum achievable intensity (Emanuel, 1995; Bister and Emanuel, 1998). The equation is

$$MPI^2 = \frac{C_k}{C_d}\frac{T_{sea} - T_0}{T_0}(k^* - k) \cong LMI^2, \tag{3.1}$$

$$\frac{C_k}{C_d} = LMI^2\left(\frac{T_{sea} - T_0}{T_0}(k^* - k)\right)^{-1}, \tag{3.2}$$

where T_{sea} is the SST under a storm, T_o is the TC outflow temperature determined by the atmospheric vertical profile, k^* is the saturation enthalpy of the sea surface, and k is the surface enthalpy in the TC environment.

The relationship between MPI and LMI (Equation (3.1)) can only be applied under limited TC conditions. For example, the relationship is not valid under the following conditions: (1) The storm moves quickly from a region with a high potential intensity to one with low potential intensity. In this case, the actual LMI can exceed the theoretical MPI because a storm needs time to adjust to its new environment. (2) The storm faces unfavorable environmental conditions, such as a strong vertical wind shear (VWS), or is influenced by the land. In this case, the actual LMI cannot approach the theoretical MPI. (3) The storm is weak. In this case, the actual LMI cannot match the theoretical MPI, given that the structure of a weak storm cannot sensitively respond to a changing environment. Therefore, by selecting only the TCs that satisfy these strict conditions, we can use the new approach to quantitatively estimate the ratio of the exchange coefficients for intense TCs (Equation 3.2).

The objectives of this study are (i) to investigate the behavior of C_k/C_d, as a function of wind speed, under severe winds, and (ii) to examine whether the new air-sea exchange flux parameterization based on current results can contribute to improving TC intensity prediction. To achieve the second objective, we designed a numerical experiment using the state-of-the-art HWRF model and applied it to idealized and real hurricane cases. Section 3.2 describes the data and methods used in this study. In Section 3.3, we show the results of the estimated C_k/C_d and

compare them with the findings of other methods. Section 3.4 shows the result of TC prediction using modified exchange coefficients in HWRF. The conclusions and discussions are provided in Section 3.5.

3.2. Data and methods

The LMI is estimated using the TC position and intensity obtained from the best track data of the JTWC for the WNP, and the NHC for the NA and the ENP. For storms that achieved their LMI more than once, the actual LMI is chosen when the storm maintains its intensity for a longer period. Since the LMI of TCs can reach the theoretical MPI under limited conditions, we select only TCs that satisfy the following conditions: (1) The representative dynamic and thermodynamic factors that relate the TC intensity, VWS, and SST should not be unfavorable for storm development. Specifically, the average VWS within a 300 km radius should be lower than 10 m s^{-1}, and the SST should be higher than 26 °C. (2) The storm should be unaffected by land; i.e., there are no landmasses within a 300 km radius of the storm center. (3) The storm should have sufficient time to adjust to the new environment as it moves; i.e., the storm translation speed should not exceed 7 m s^{-1}. (4) The storm should keep quasi-steady conditions at the LMI stage; i.e., it should maintain its strength for at least 12 h after reaching the LMI. (5) The environmental conditions along the storm track should not significantly change for at least 12 h after the storm achieves its LMI. (6) The storm should have an intensity of at least Category 2 (above 40 m s^{-1}). From the total of 2,255 TCs that occurred in the NA, ENP, and WNP basins between 1980 and 2015, which is the period when the TC intensity can be accurately estimated using geostationary satellites, 84 TCs satisfied the above conditions (Figure 3.2, Table 3.1).

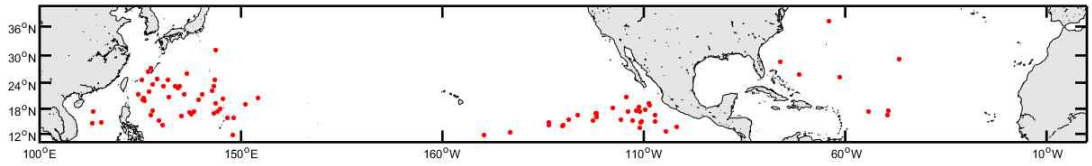

Figure 3.2. Locations at LMI for TCs (total 84) selected for C_k/C_d parameterization over WNP, ENP, and NA basins in 1980–2015.

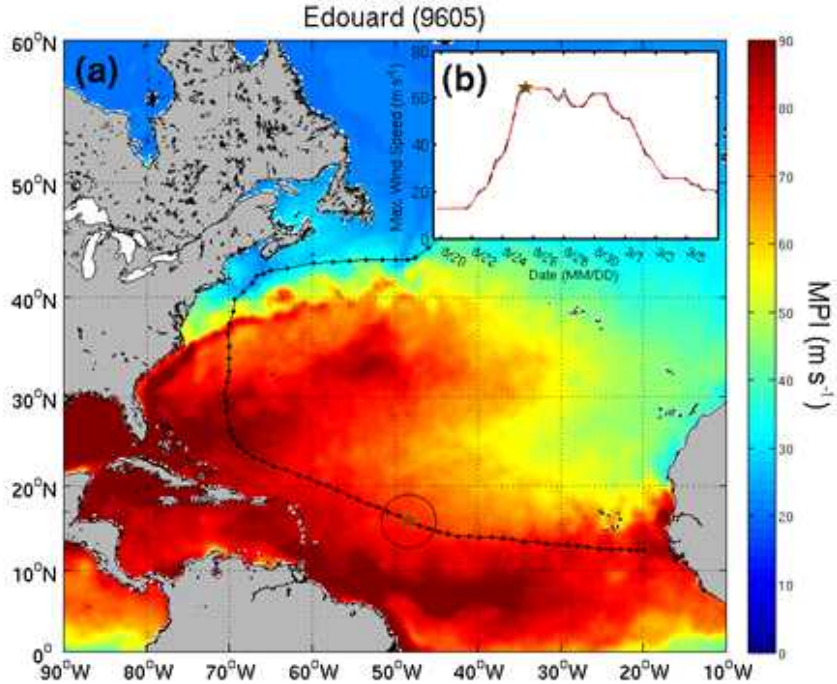

Figure 3.3. Example of estimating MPI and LMI for Hurricane Edouard in 1996. (a) Spatial distribution of theoretical MPI on August 20, 1996 and track of hurricane Edouard (black line with dots). (b) Variations of MWS during lifetime of Hurricane Edouard. Here, the time of LMI (star symbol) is determined when the storm has a peak value at the time series of the smoothed MWS (12 h moving average, red lines) and maintains its strength within ± 2.6 m s $^{-1}$ for at least 12 h after the LMI is archived. The MPI at each point is estimated by averaging the MPIs within 300 km of the storm center.

Table 3.1. TC, period, maximum sustained wind speed (kt), minimum central pressure (hPa), and the Saffir-Simpson wind scale for 84 selected TCs over the WNP, ENP, and NA basins over 1980–2015.

Basin	Year	Storm
AL (8)	1995	LUIS (13L)
	1996	EDOUARD (05L)
	1996	FRAN (06L)
	1996	HORTENSE (08L)
	1997	ERIKA (07L)
	2001	FELIX (07L)
	2003	JUAN (15L)
	2010	IGOR (11L)
EP (30)	1982	JOHN (10E)
	1982	NORMAN (14E)
	1982	SERGIO (18E)
	1983	ADOLPH (01E)
	1984	FAUSTO (06E)
	1984	POLO (17E)
	1985	TERRY (19E)
	1987	OTIS (15E)
	1987	RAMON (17E)
	1988	LANE (12E)
	1990	JULIO (13E)
	1990	MARIE (16E)
	1991	JIMENA (12E)
	1991	KEVIN (13E)
	1992	CELIA (04E)
	1992	FRANK (07E)
	1993	GREG (08E)
	1993	HILARY (09E)
	1994	EMILIA (05E)
	1997	NORA (16E)
	1998	HOWARD (09E)
	1999	EUGENE (08E)
	2000	ALETTA (01E)
	2001	GIL (08E)
	2001	JULIETTE (11E)
	2002	DOUGLAS (05E)
	2005	KENNETH (11E)
	2006	DANIEL (05E)
	2006	HECTOR (09E)
	2010	DARBY (05E)
WP (46)	1980	DINAH (27W)
	1982	PAT (04W)
	1982	BESS (11W)
	1982	IRVING (18W)
	1982	JUDY (19W)

	1982	KEN (20W)
	1982	MAC (23W)
	1986	BEN (16W)
	1987	THELMA (05W)
	1987	FREDA (13W)
	1987	IAN (17W)
	1988	HAL (14W)
	1988	NELSON (20W)
	1988	ODESSA (21W)
	1990	MIKE (27W)
	1990	RUSS (31W)
	1991	WALT (04W)
	1991	PAT (24W)
	1991	SETH (26W)
	1992	COLLEEN (26W)
	1993	ROBYN (13W)
	1994	WALT (10W)
	1994	WILDA (35W)
	1995	OSCAR (17W)
	1995	WARD (26W)
	1995	ZACK (28W)
	1996	KIRK (13W)
	1996	YATES (28W)
	1997	WINNIE (14W)
	2000	KIROGI (05W)
	2001	KONG-REY (09W)
	2001	MAN-YI (12W)
	2001	NARI (20W)
	2001	KROSA (24W)
	2002	RAMMASUN (09W)
	2002	FENGSHEN (12W)
	2002	RUSA (21W)
	2004	TINGTING (11W)
	2005	TALIM (13W)
	2006	CHANCHU (02W)
	2007	MAN-YI (04W)
	2008	NAKRI (06W)
	2010	CHABA (16W)
	2012	TEMBIN (15W)
	2012	JELAWAT (18W)
	2013	FRANCISCO (26W)

The MPI is calculated using Emanuel's potential intensity program ('pcmin' code) based on Equation 3.1, in which a scaling factor (VREDUC) of 0.8 is used to reduce the gradient wind to the surface wind. For the MPI calculation, the atmospheric input is obtained from the daily atmospheric temperature and humidity profile data from the Modern-Era Retrospective Analysis for Research and Applications (MERRA) dataset in a 1.5° × 1.5° longitude-latitude grid. The SST under the storm (T_{sea}) is obtained from oceanic reanalysis data from the NCEP Global Ocean Data Assimilation System (GODAS), which provides pentad ocean subsurface temperatures at 40 geometric depth levels in a 1.5° × 0.333° longitude-latitude grid for 1980 to present. The depth-averaged temperatures (T_{80}) from the surface to a depth of 80 m are calculated by averaging the GODAS data from the surface to the 80 m depth after the ocean temperature is interpolated to a 1 m depth interval. The MPI, including enthalpy (k and k*) at the LMI location, is calculated by averaging the values within a 300 km radius of the storm center using prestorm conditions (3 days before LMI) (Lin et al., 2013) (Figure 3.3). To test the sensitivity of the SST data to the C_k/C_d calculation, we calculate additional MPIs using Group for High-Resolution Sea Surface Temperature (GHRSST) data, which are produced daily at the Canadian Meteorological Centre with a spatial resolution of 0.2° × 0.2°. Since the GHRSST data are only from September 1991, the MPIs are derived only for the 38 TC cases that satisfy the previously described conditions from 1991 to 2015.

Numerical prediction experiments for the idealized and real TC cases are conducted using the HWRF to test the new air-sea exchange flux parameterization. In this study, we use the 2017 HWRF version, which has a 3 km spatial resolution. Further details regarding the input data and model setup are described in Biswas et al. (2018). The International Best Track Archive for Climate Stewardship (IBTrACS), produced by the NHC and the JTWC, is used to verify the TC forecasts (Knapp et al., 2010).

3.3. New parameterization of C_k/C_d

Figure 3.4a shows a scatter plot of C_k/C_d as a function of LMI, which is estimated using Equation (3.2) for the 84 selected TCs. The estimated C_k/C_d ranges from 0.2 to 1 for wind speeds of 40–75 m s^{-1}, and it clearly increases with the MWS. Based on these results, we estimate the wind dependency of the ratio using a regression function (Figure 3.4a) and apply this, instead of the traditionally used constant C_k/C_d (unity), to Equation (3.1). As a result, the correlation between the observed LMI and the theoretical MPI significantly increases from 0.34 to 0.86. The error decreases from 29.3 m s^{-1} to 5.4 m s^{-1} (refer to the blue and red dots shown in Figure 3.4b, respectively, in Figure 3.4b). Therefore, the increasing C_k/C_d with wind speed at strong winds above 40 m s^{-1} may help estimate a realistic intensity of intense TCs (this possibility is examined in the next section). A comparison of our mean C_k/C_d values (red symbol and line in Figure 3.5) with those in earlier studies, especially at wind speeds above 40 m s^{-1}, shows that our results are generally within the range of Bell et al. (2012) but much smaller than those of Emanuel (1995). Figure 3.6 shows the prestorm SST–based C_k/C_d obtained using GHRSST and GODAS. The similar pattern between the two datasets suggests that the present method is not highly sensitive to the SST data selection and the considered analysis period.

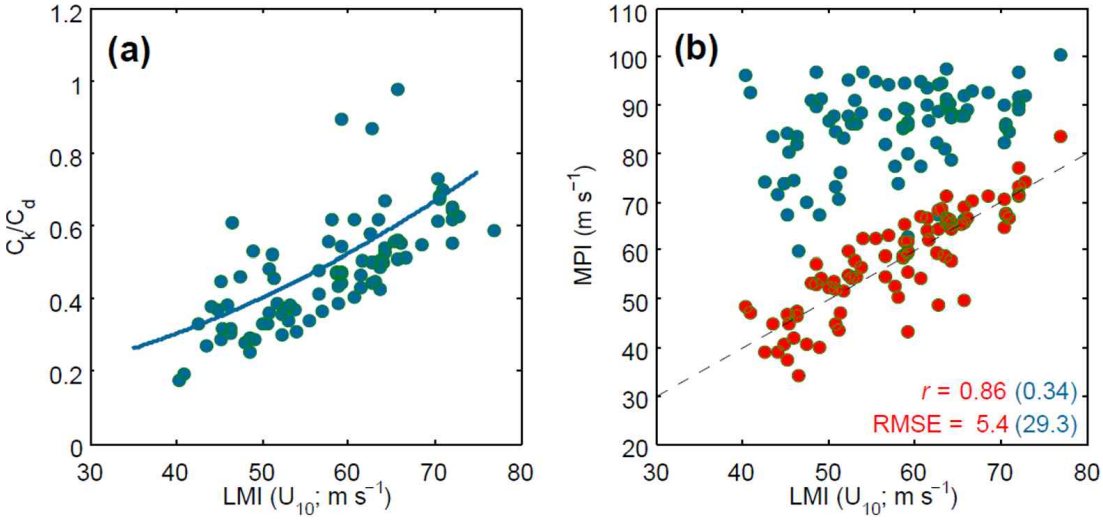

Figure 3.4. Scatter plot of C_k/C_d and theoretical MPI against LMI (i.e., MWS at 10 m, U_{10}) for major TCs. (a) Scatter diagram of C_k/C_d and its linear fit (blue line, 1.1013e-04 + 0.1281) onto LMI. (b) Comparison of MPI calculated using unity (traditional way, blue dots) and linear fit (red dots) estimated by present approach for C_k/C_d. Correlation coefficients (r) and root mean square errors (RMSEs, m s^{-1}) are shown in the lower right corner.

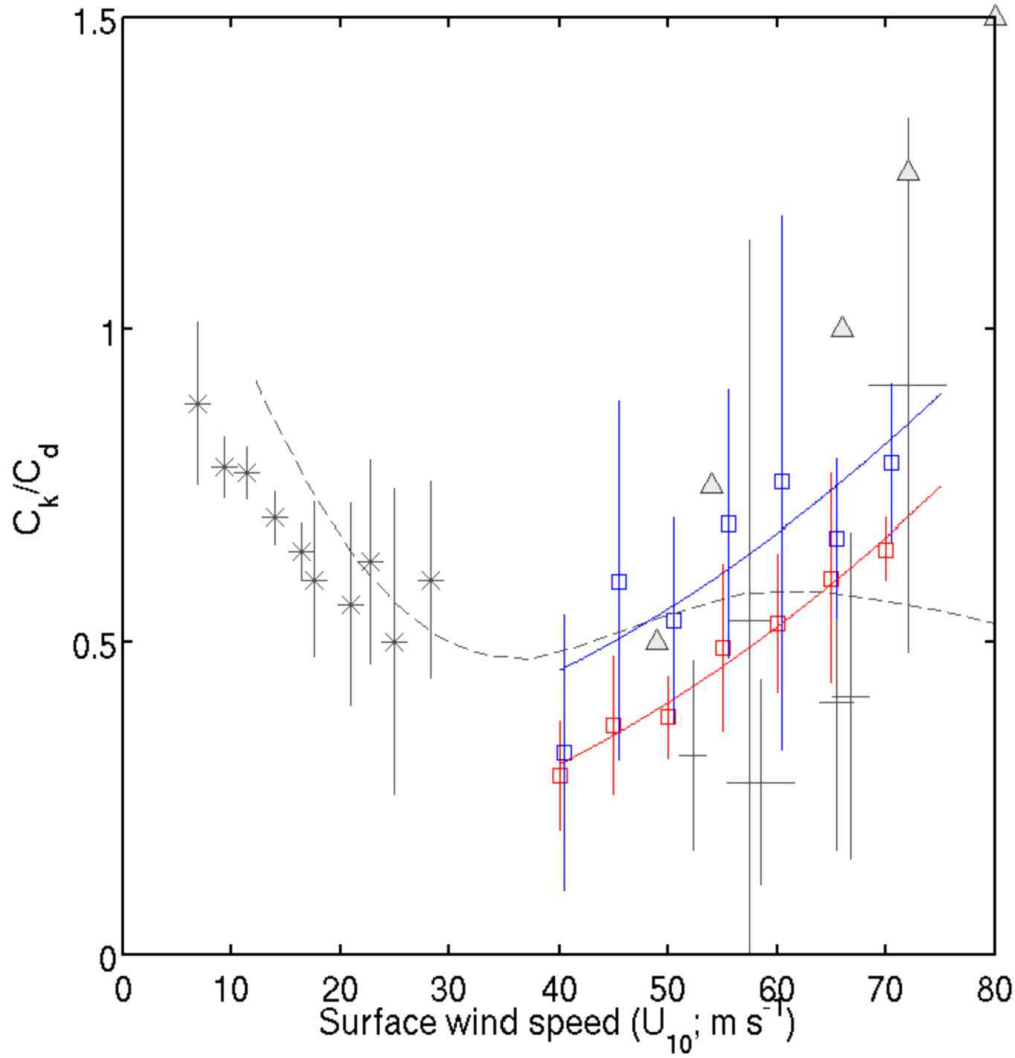

Figure 3.5. Dependence of C_k/C_d on U_{10} based on prestorm SST and depth-averaged temperatures compared with previous studies. The red and blue squares indicate the mean values of C_k/C_d within each 5 m s^{-1} interval of wind speed, estimated using prestorm SST and depth-averaged temperatures (T_{80}), respectively. The color lines and error bars indicate linear fits and one standard deviation in the bins (the linear fit of the blue line is 1.0943e-04 + 0.2799). The dashed gray lines indicate data adapted from Soloviev et al. (2014), and the gray triangles indicate data adapted from Emanuel (1995). The mean and 95% confidence intervals of diverse laboratory and measurement results (Bell et al., 2012; DeCosmo et al., 1996; Haus et al., 2010; Zhang et al., 2008) are shown in gray asterisks and solid lines.

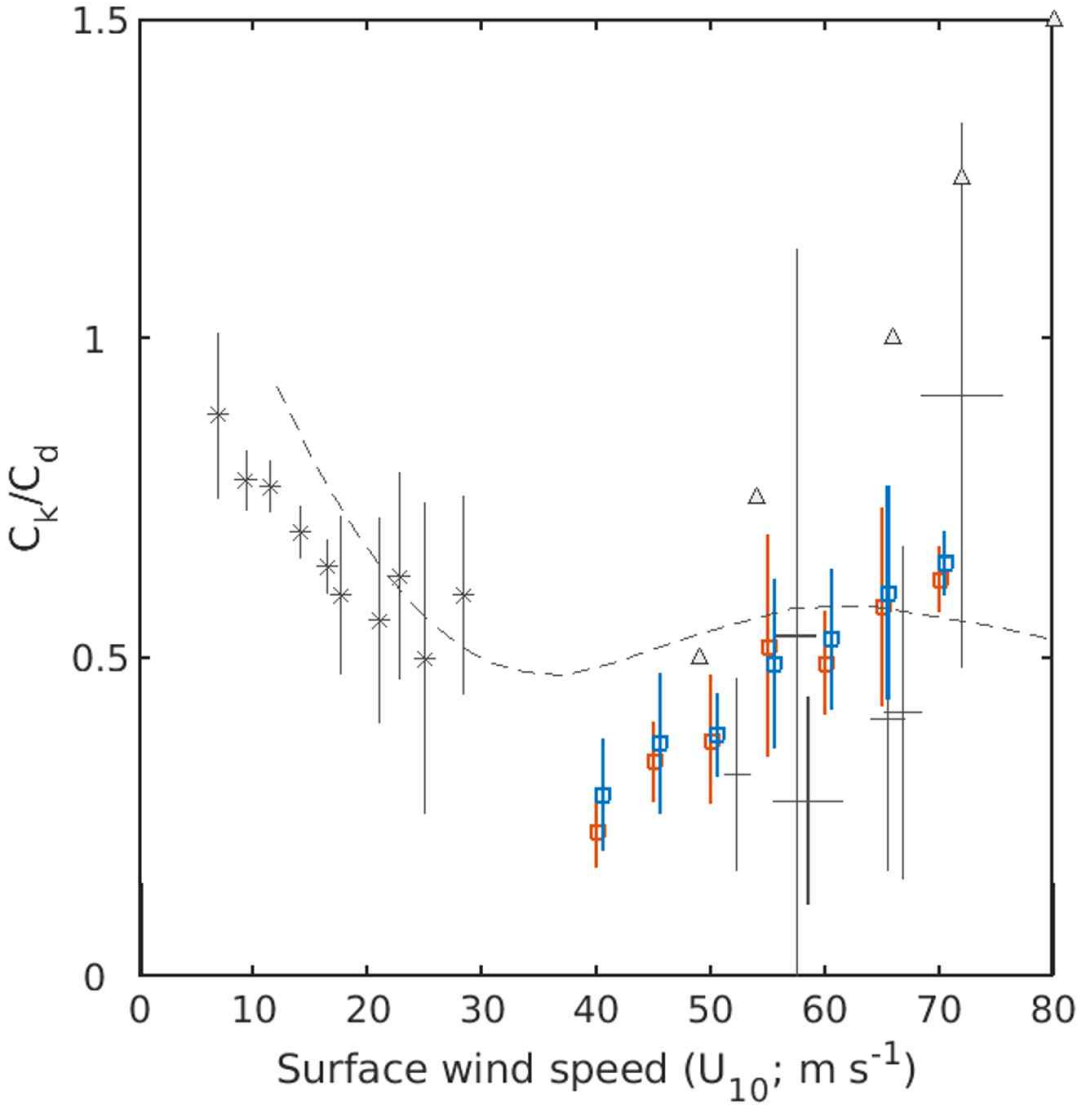

Figure 3.6. Sensitivity of SST data to calculation of C_k/C_d. Comparison of C_k/C_d estimated using prestorm SST from GHRSST (red) and GODAS (blue) against U_{10}. The squares indicate the mean values of C_k/C_d within each 5 m s^{-1} interval of wind speed. The error bars represent one standard deviation. The dashed gray lines indicate data adapted from Soloviev et al. (2014), and the gray triangles indicate data adapted from Emanuel (1995). The mean and 95% confidence intervals of diverse laboratory and measurement results (Bell et al., 2012; DeCosmo et al., 1996; Haus et al., 2010; Zhang et al., 2008) are shown in gray asterisks and solid lines.

In the original MPI method, T_{sea} is calculated using the prestorm SST (Emanuel, 1988; Emanuel, 1995; Holland, 1997; Wang and Wu, 2004), which does not include the contribution of TC-induced SST cooling. The MPI in Figure 3.4 is also estimated using the prestorm SST. A recent study suggested that prestorm depth-averaged (averaged from the surface mixing depth down to the expected TC-induced mixing depth) ocean temperatures are more appropriate for calculating the MPI than the prestorm SST (Lin et al., 2013). This is based on in situ air-deployed ocean-atmosphere measurement pairs collected during the Impact of Typhoons on the Ocean in the Pacific (ITOP) program. In particular, the depth-averaged temperature (T_{80}) from the surface to a depth of 80 m has been identified as the most appropriate index related to TC intensity under a wide range of major TC conditions (Price, 2009; Lin et al., 2013), although the TC-induced mixing depth also depends on the TC translation speed, size, and intensity and the upper ocean thermal structure (Price et al., 1994; Lin et al., 2009; Price, 2009).

Figure 3.5 compares the C_k/C_d estimated using the prestorm SST and T_{80} (blue symbol and line, respectively). The most distinct discrepancy between the two results is an overall increase in the mean C_k/C_d values and their standard deviations when T_{80} is used. This result implies that a higher C_k/C_d value is required for the storm to reach a certain intensity when the effect of storm-induced surface cooling on the MPI calculation is considered. It also suggests that numerical experiments without negative ocean feedback may lead to a different conclusion about the behavior and magnitude of C_k/C_d (Montgomery et al., 2010; Bryan, 2012; Green and Zhang, 2013; Li et al., 2016). A large increase in the standard deviation of T_{80} can be explained by the fact that the depth-averaged temperature can vary significantly due to different factors, such as the mixing depth and subsurface structure. A comparison of the two mean C_k/C_d values with those in earlier studies at wind speeds above 40 m s^{-1} shows that our results are generally higher than those of Bell et al. (2012) for all covered wind speeds except the 72.5 m s^{-1} bin, where the values are similar. At wind speeds of 40–55 m s^{-1}, the T_{80}-based C_k/C_d regression

line generally agrees with that of Soloviev et al. (2014) in terms of the positive slope of C_k/C_d (blue and dashed lines in Figure 3.5). However, at wind speeds above 55 m s^{-1}, Soloviev et al.'s ratio decreases, while our calculated ratio increases with wind speed.

The continuously increasing trend of C_k/C_d at high winds is qualitatively consistent with previous results (Emanuel, 1995; Andreas, 2011; Bao et al., 2011; Bell et al., 2012; Richter & Stem, 2014). The increasing trend of C_k/C_d at high winds is possibly due to increasing C_k (Mueller and Veron, 2014) and/or decreasing C_d (Powell et al., 2003; Jarosz et al., 2007; Vickery et al., 2009; Soloviev et al., 2014). Some previous studies attribute this tendency to the effect of sea spray (Andreas, 2011; Bao et al., 2011). As wind speed increases, the mean droplet size and the mass flux of sea spray increase. The C_k/C_d trend of continuously increasing at extreme wind speeds above 40 m s^{-1} may support the importance of spray-mediated air-sea enthalpy and momentum fluxes under TCs. However, the precise mechanisms responsible for this trend remain unknown.

The C_k/C_d presented here may have significant implications for improving operational TC prediction, which currently tends to severely underestimate the intensity of major hurricanes. The HWRF uses C_k/C_d parameterization of the curved-fitting to available field measurements from recent observations (Biswas et al., 2018). The C_k/C_d value used in the HWRF may be too low at wind speeds above 60 m s^{-1}. In fact, the C_k/C_d from our T_{80}-based parameterization becomes greater with increasing wind speed compared with the estimates of Soloviev et al. (2014). This suggests that using the new C_k/C_d in operational models may help reduce the negative bias in TC intensity prediction for major hurricanes, as demonstrated in the next section.

3.4. Effects of new C_k/C_d parameterization on TC intensity prediction

To examine the impact of the new parameterization of enthalpy-momentum exchange coefficients, we perform three sets of numerical experiments using the HWRF. In the first experiment (CTRL), we use the original C_d parameterization of the HWRF (version 3.9a), in which C_d and the surface roughness lengths (z_o) level off at 50 m s^{-1} (black line in Figures 3.7a, b). This is based on Soloviev et al. (2014) with slight modifications (Biswas et al., 2018). The other two experiments employ the increasing C_k/C_d trend derived from our T_{80}-based parameterization. The increasing C_k/C_d ratio can mean that C_d decreases, or C_k increases, or both C_d decreases and C_k increases. It is difficult to modify both C_d and C_k at the same time because we cannot deduce accurately the ratio, and limited computation resources are not enough to test every possible combination of C_k and C_d. Therefore, to investigate the individual impact of the coefficients on TC intensification, we employ two types of increasing C_k/C_d parameterization: 1) decreasing C_d with nearly constant C_k (Cd_DC, red line in Figures 3.7a, b; CTRL, back line in Figures 3.7c, d) and 2) increasing C_k with the original C_d (Ck_IC, blue line in Figures 3.7c, d; CTRL, back line in Figures 3.7a, b).

Table 3.2. Numerical experimental design to investigate the effect of air-sea flux parameterizations on TC simulations using HWRF.

Experimental Name	Air-sea flux parameterizations above 50 m s^{-1}	
	C_d	C_k
CTRL	Original HWRF (constant)	Original HWRF (nearly constant)
Cd_DC	Decreasing C_d	Original HWRF (nearly constant)
Ck_IC	Original HWRF (constant)	Increasing C_k

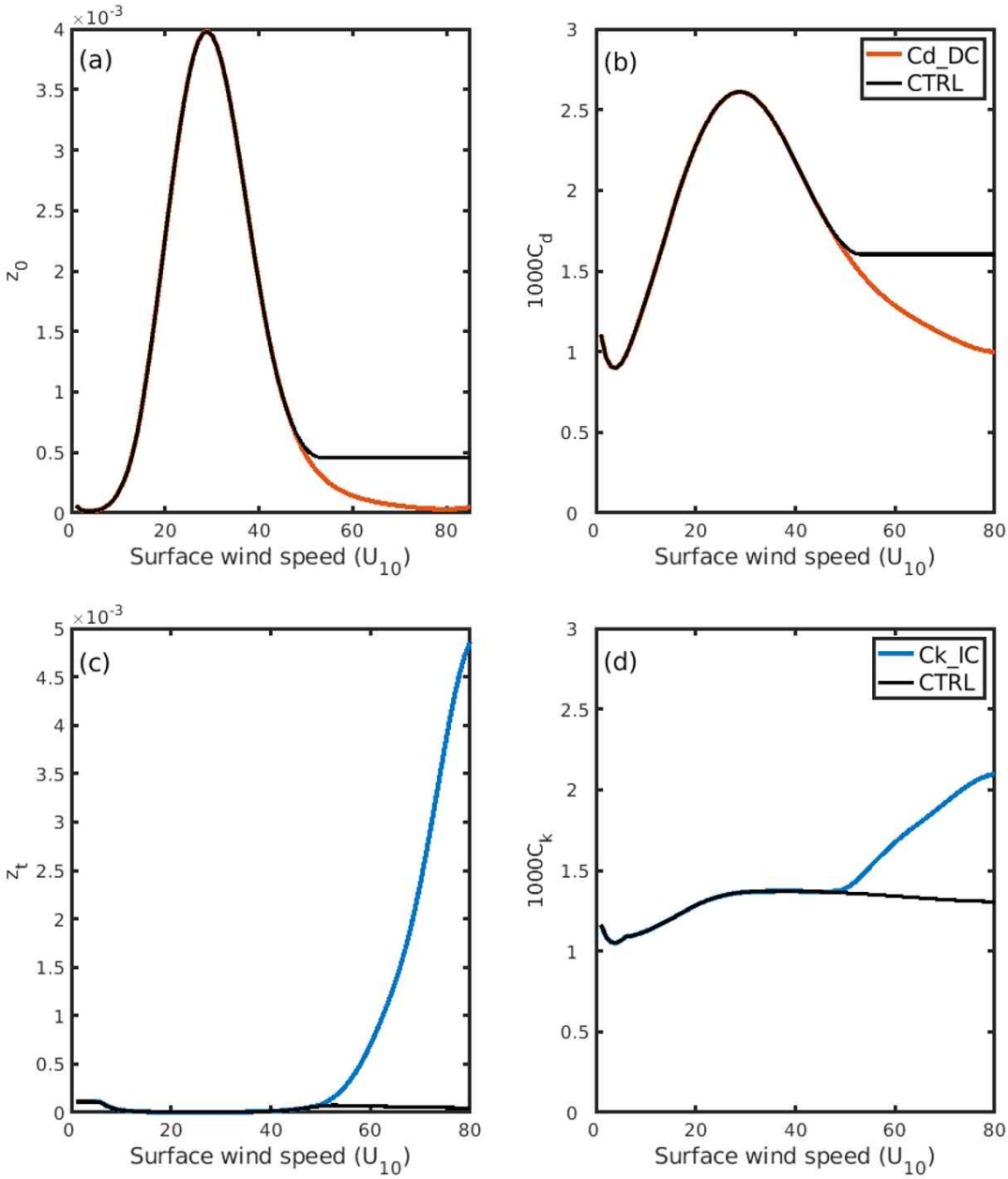

Figure 3.7. Parameterization of (a) roughness lengths for momentum z_o, (b) drag coefficient C_d, (c) roughness lengths for heat and humidity, and (d) heat exchange coefficient C_k as a function of 10-m wind speed, as used in the CTRL, Cd_DC and Ck_IC experiments (CTRL, black curve; Cd_DC, red curve; Ck_IC, blue curve).

The effects of the modified flux parameterizations on TC simulations are investigated using three sets of experiments—CTRL, Cd_DC, and Ck_IC (Table 3.2)—for idealized and real TC cases, in which all experiments are identical except that different surface exchange coefficients are used. We first investigate the sensitivity of parameterization in an idealized uncoupled experiment where the atmospheric model receives no feedback from the ocean. The experiment was conducted using an idealized HWRF framework, which is configured for the operational HWRF triple domain configuration with a grid spacing of 13.5-, 4.5-, and 1.5 km (Biswas et al., 2018). The initial intensity of the idealized vortex was 20 m s^{-1} and the radius of maximum winds was 90 km, which is embedded in a quiescent ambient. The base-state temperature and humidity profile are based on Jordan's Caribbean sounding (Gray et al., 1975). The SST is constant in time and space (304.75 K), and no land is present in the domain (Figure 3.8a).

Next, a series of idealized coupled TC simulations are conducted to investigate how the new C_k/C_d parameterization under high winds modulates the air-sea interactions and how it affects TC intensification. A three-dimensional ocean model, Message Passing Interface Princeton Ocean Model-Tropical Cyclone (MPIPOM-TC), is embedded into the HWRF (HWRF-MPIPOM-TC). A coupler developed by NCEP serves as a hub for MPI communications between the HWRF atmosphere and MPIPOM-TC by which the surface fluxes and SSTs are exchanged between the HWRF atmospheric grids and the MPIPOM-TC grids. The initial ocean fields used for this experiment are horizontally uniform and based on temperature and salinity profiles as shown in Figure 3.8b.

In addition to the idealized experiments, two real-case experiments for Hurricane Irma (2017) and Typhoon Mangkhut (2018) are conducted. In this experiment, as in the idealized cases, the three parameterizations in Table 3.2 are also tested using a coupled model. Each simulation is integrated for 126 hours, and the output is saved every 3 h. As described earlier, the three sets of experiments are identical except for using different surface exchange coefficients.

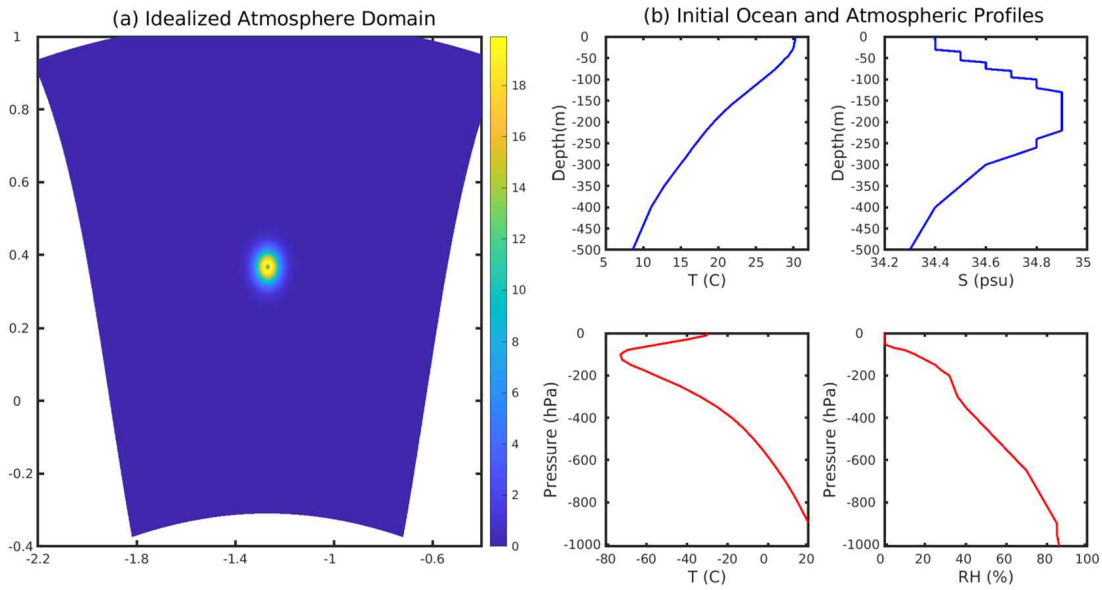

Figure 3.8. (a) Model domain for idealized experiments. Colors show wind speed with the initial vortex situated at the center of the domain. (b) Initial oceanic and atmospheric profiles used in idealized experiments. All initial temperature and salinity profiles for ocean and initial temperature and humidity sounding are horizontally uniform.

Figure 3.9 shows the time series of 48-h moving averaged MWS from three experiments in both idealized uncoupled and coupled experiments. Here, the TC intensity changes for the three different parameterizations have a similar trend during the first 24 h when the MWS has not yet reached 50 m s^{-1}. This is because the C_d and C_k parameterizations at wind speeds below 50 m s^{-1} are the same in all three experiments. However, after 24 h, the Cd_DC and Ck_IC simulations persistently produce a greater MWS than the CTRL simulation. The TC intensity in the coupled model is lower in the uncoupled experiment due to the negative feedback from the ocean. Interestingly, in uncoupled simulations, the MWS in the Cd_DC and Ck_IC are similar to each other at all forecast times (Figure 3.9a), while, in coupled experiments, Cd_DC simulates a stronger than Ck_IC by up to 14 m s^{-1} (Figure 3.9b). To examine why the intensity differs between the Cd_DC and Ck_IC in coupled experiments, we conducted six idealized ensemble experiments forced with

different combinations of atmospheric initial and boundary conditions and analyzed TC-induced sea surface temperature cooling (SSC) and air-sea humidity difference ($\Delta Q = Q_s - Q_a$). The SSC is calculated as the SST of each forecast time from 6 h to 120 h minus the SST of the initial forecast time, in which the SST is averaged within 50 km from the TC center for each forecast time.

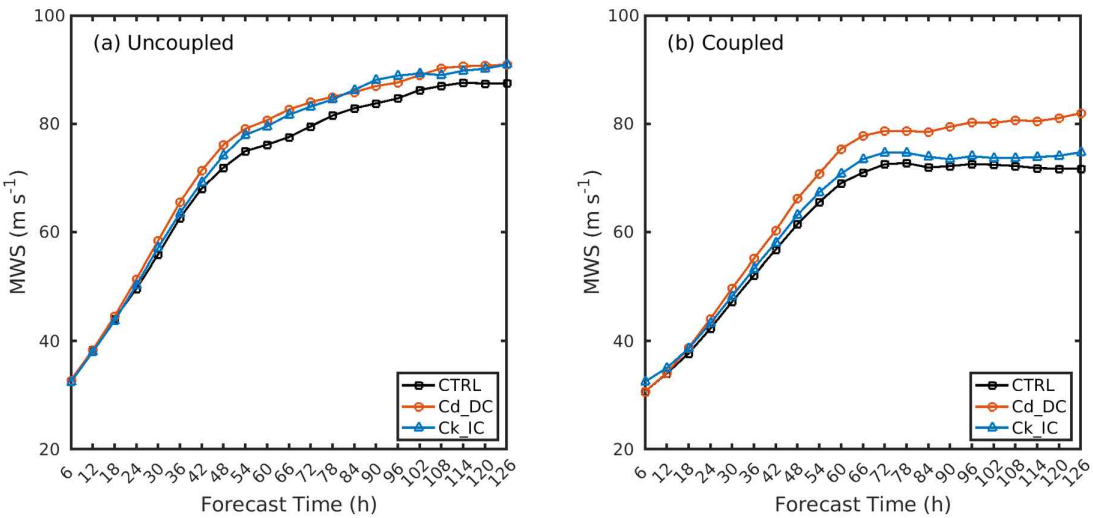

Figure 3.9. Time series of maximum wind speed (m s $^{-1}$) for three simulations of idealized uncoupled (a) and coupled (b) experiments. Wind speeds are smoothed by a 48-h moving average.

The SSC for all three experiments tends to increase as the MWS increases. A closer look reveals that the SSC from both CTRL and Ck_IC is greater than that of Cd_DC (particularly, the difference is statistically significant above the 99 % confidence level between 60 m s^{-1} and 80 m s^{-1}) (Figure 3.10). Because the wind stress is proportional to the C_d times the wind speed squared, a decreased C_d reduces the momentum flux into the ocean, inhibiting vertical mixing of the upper ocean. Consequently, SSC in Cd_DC experiment is reduced, thereby increasing heat fluxes that contribute positively to TC intensification (Figure 3.11). Based on the bulk aerodynamic formula, increased C_k also contributes to the increase of heat fluxes

favoring for TC intensification. Both decreased C_d and increased C_k under high winds can positively contribute to the TC intensification; however, the contribution of C_d is more significant than that of C_k because C_d affects not only frictional dissipation but also the heat flux in high winds.

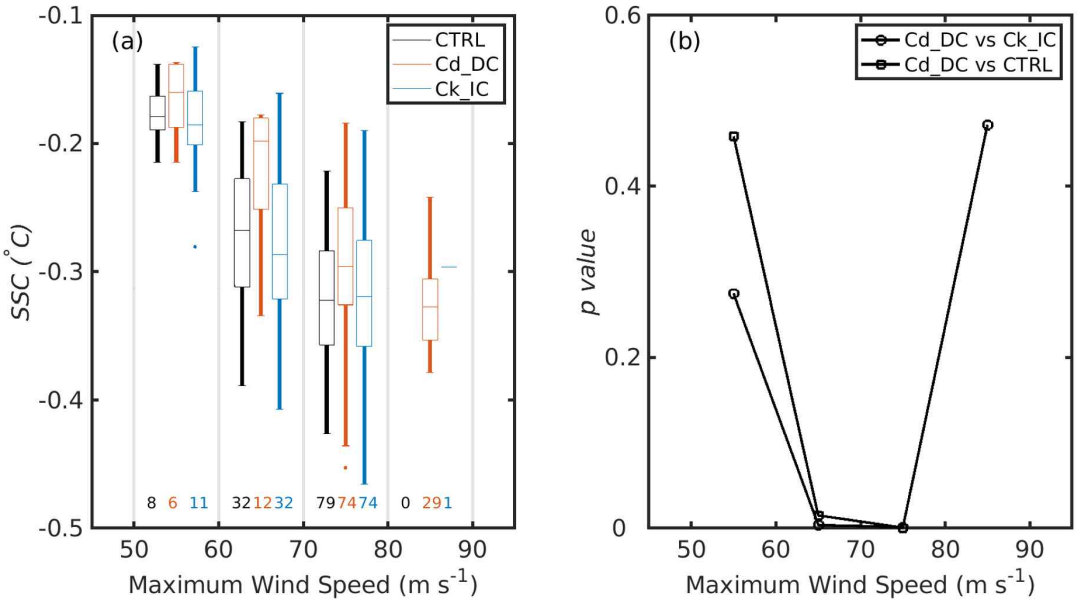

Figure 3.10. (a) Boxplots for sea surface cooling (°C) as a function of MWS at each 10-m s^{-1} interval. The lines denote the median values, and the box covers the 25%-75% quantile. The bars show the minimum and maximum values, the points show the outliers. Colors indicate results for CTRL (black), Cd_DC (red) and Ck_IC (blue). The numbers above the x axis denote the assigned TC case number for each experiment. (b) The p value for the SSC differences between Cd_DC and Ck_IC (solid open circle) and between Cd_DC and CTRL (solid open square) based on Student t-test.

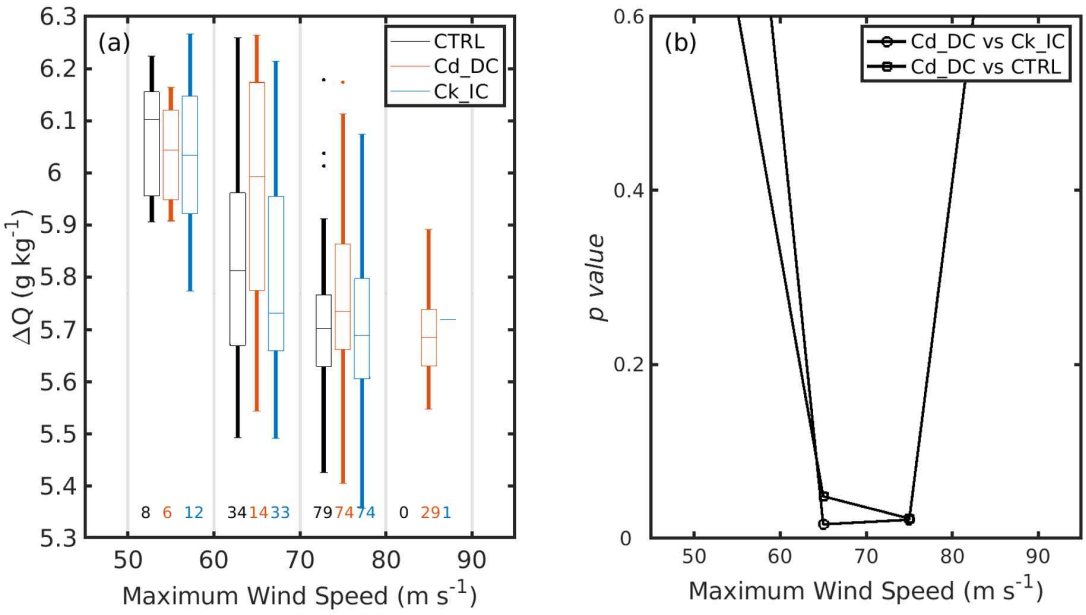

Figure 3.11. Same in Figure 3.10, but for the air-sea moisture difference.

We conduct a total of 40 real-case predictions (6 h intervals) for two Category 5 TCs: Hurricane Irma (1200 UTC, August 30, 2017, to 1200 UTC, September 5, 2017, in NA) (Figure 3.12a) and Typhoon Mangkhut (0000 UTC, September 8, 2018, to 1200 UTC, September 11, 2018, in WNP) (Figure 3.12b). The prediction results are evaluated for TC intensity (i.e., MWS) above 50 m s^{-1} with different parameterizations of surface exchange coefficient in three experiments. Statistics show that Cd_DC outperforms both CTRL and Ck_IC in terms of the mean absolute error and bias in the intensity prediction of Irma and Mangkhut (Figure 3.13). For Irma, all absolute errors increase rapidly with the forecast lead time up to 48 h, but they level off thereafter. The difference between the three experiments becomes evident after 48 h, in which the error of Cd_DC is smaller by about 15% than that of CTRL after 48 h (Figure 3.13a). The reduction in error can be mainly explained by the bias differences between the experiments. That is, the negative bias of Cd_DC is smaller by 19% than that of CTRL after 48 h (Figure 3.13c). In contrast to Cd_DC, Ck_IC errors are slightly lower or similar to the CTRL errors. For Ck_IC, the mean absolute error after 48 h is reduced by about 3 % compared to the CTRL. For the case of Mangkhut, the bias and errors of Cd_DC are significantly reduced at most forecast lead times (Figures 3.13b, d). In particular, for all forecast leads, Cd_DC reduced the absolute error on average by ~32% compared to CTRL. On the other hand, Ck_IC forecasts are not significantly improved compared to CTRL. These results are similar to those of Irma, implying that decreasing C_d can reduce the TC intensity error more effectively than increasing C_k under high winds.

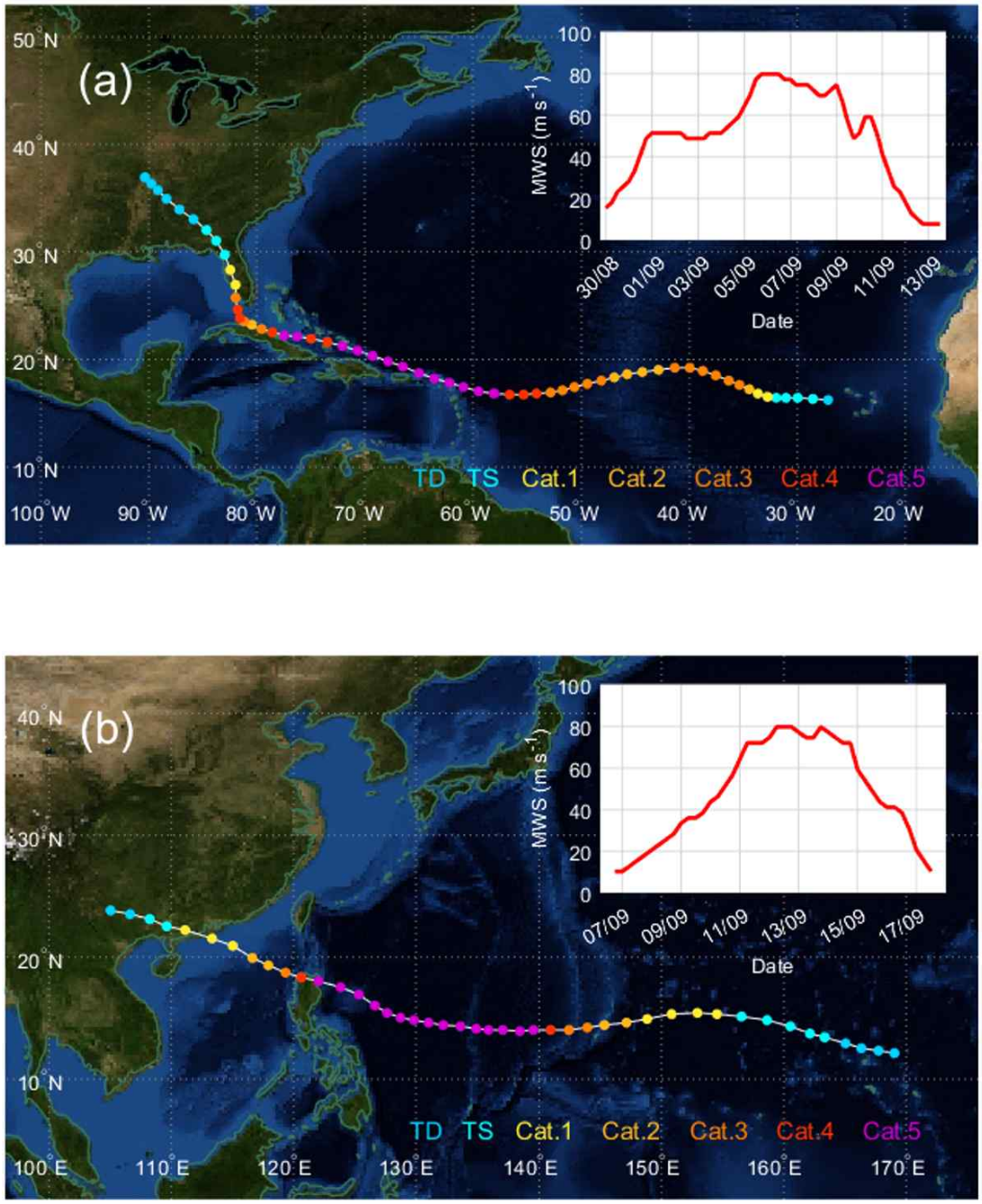

Figure 3.12. (a) Hurricane Irma over North Atlantic in 2017 and (b) Typhoon Mangkhut over western North Pacific in 2018. The best-track positions and maximum wind speeds (in the box) are shown at 6-h intervals along with the intensity of the Saffir-Simpson wind scale (solid circle).

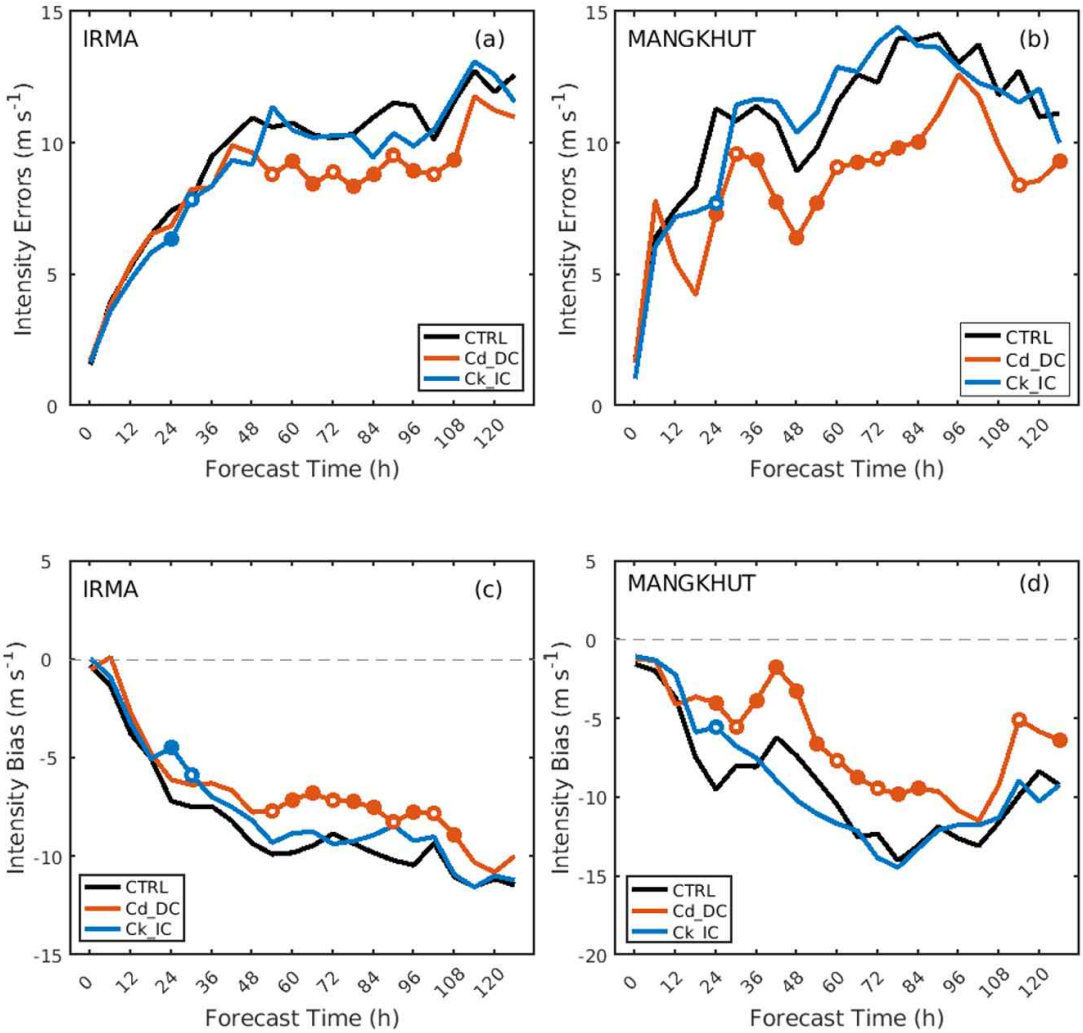

Figure 3.13. Comparisons of mean absolute error (a, b) and mean bias (c, d) against forecast lead time for three experiments, CTRL (black line), Cd_DC (red line) and Ck_IC (blue line), for Irma (a, c) and Mangkhut (b, d). Red (blue) closed [open] circles indicate that the binned value for Cd_DC (Ck_IC) is significantly improved than for CTRL at the 99 % [95 %] confidence level (Student's *t*-test).

In the Cd_DC experiment, the constant C_d at winds above 50 m s^{-1} is only replaced by a C_d that continues to decrease with increasing wind speed. This suggests that such improvement in intensity prediction for the two TCs is attributed to the reduction in C_d. To summarize, the decrease in C_d at high winds provided two favorable conditions for TC intensification: (1) a decrease in frictional dissipation at the air-sea interface and (2) and an increase of air-sea enthalpy (latent plus sensible heat) fluxes due to the reduced SST cooling caused by the decrease in momentum flux into the sea. Again, this emphasizes that the decrease in C_d at high winds might play a key role in improving intensity prediction for major TCs.

3.5. Discussion and conclusion

We present a new parameterization of C_k/C_d at high wind speeds above 40 m s^{-1} that uses the relationship between the observed LMI and theoretical MPI. This new parameterization shows that C_k/C_d increases with wind speed. To investigate whether the proposed parameterization can improve TC intensity prediction, we conduct triplet numerical experiments using the HWRF model, called CTRL, Cd_DC and Ck_IC. The first uses C_d that is constant at wind speeds above 50 m s^{-1}, the second uses C_d that decreases continuously with wind speed (as C_d decreases, C_k/C_d increases with wind speed due to the constant C_k used in the HWRF model) and the last uses C_k that increases continuously with wind speed (as C_k increases, C_k/C_d increases with wind speed due to the nearly constant C_d above 50 m s^{-1} used in the HWRF model). Idealized uncoupled and coupled experiments, Ck_IC and Cd_DC show stronger TC intensity than CTRL. However, there is no significant difference in TC intensity between Ck_IC and Cd_DC in the uncoupled simulations, while the intensity of Cd_DC appears to be stronger than Ck_IC in the coupled simulations. The results show that the decreased C_d not only reduces frictional dissipation but also causes a reduction in the air-sea momentum flux, consequently inhibiting SSC. The extra energy supplied by the reduced SSC in the Cd_DC experiment simulated a stronger TC than in the CK_IC experiment. Similar results are found in the numerical simulations of two category-5 TCs, Hurricane Irma (2017) and Typhoon Mangkhut (2018). Both Cd_DC and Ck_IC reduced negative bias in TC intensity prediction, however, only the former result was statistically significant. This suggests that decreasing C_d may be more effective than increasing C_k in reducing the underestimation of TC intensity in the coupled model simulation.

Efforts have been made in recent years to find the optimal parameterization of air-sea exchange coefficients on TC evolution using an atmosphere-ocean coupled modeling system (Chen et al., 2018; Liu et al., 2022). Using the atmosphere-ocean

coupled experiment, Chen et al. (2018) performed a sensitivity test of three C_d parameterizations (increase, decrease, and level off in high winds) for Hurricane Katrina. Their study indicated that the use of a momentum flux parameterization with decreasing C_d and default C_k (Chen and Yu 2016; C_k/C_d ratio increased) in high winds improve the accuracy of TC intensity prediction for very strong wind. Liu et al. (2022) performed sensitivity experiments of C_d parameterization using a coupled model and compared the sea surface cooling reproduced in the model with buoy data. They found that the heat flux was significantly affected by the C_d-induced sea surface cooling effect rather than the change in wind speed in the model results. Their main findings are consistent with ours regarding the importance of the use an atmosphere-ocean coupled model, resulting in better understanding of the flux exchange between TCs and the ocean.

In this study, we estimate C_k/C_d under the most intense TCs using the MPI approach, which has some limitation that need to be discussed. First, technically, the MPI defined by Equation 3.1 is the axisymmetric gradient wind at the top of the boundary layer, while the LMI is the maximum 1-minute sustained 10 m surface wind, which is a different metric from the MPI (Emanuel and Rotunno, 2011). This study uses a VREDUC factor of 0.8 in the MPI calculation using Emanuel's 'pcmin' code to reduce the maximum gradient wind (Vmax) to the surface wind. However, a possible scenario is that C_k/C_d is constant, but the mixing of momentum in the boundary layer changes as a function of the intensity such that VREDUC is variable instead of constant in a comparison of MPI and LMI. This is based on the relationship between C_k/C_d and Vmax, which can be affected by the parameterization of turbulence in an axisymmetric model (Bryan and Rotunno, 2009). If the identified relationship is actually between the gradient wind and surface wind as a function of wind speed, both 40 m s^{-1} and 80 m s^{-1} surface winds should have the same gradient wind as that of 80 m s^{-1}, since our regression function of C_k/C_d (blue line in Figure 3.5) shows ~0.5 at 40 m s^{-1} and ~1.0 at 80 m s^{-1}. This cannot happen in reality, as the TC should keep a similar magnitude of the relationship between the

gradient wind at the top of the boundary layer and the surface wind.

Second, when the VREDUC factor of 0.8 reduces the gradient wind to the surface wind, the reduced values are not constant; they are a function of wind speed. The factor reduces 80 m s^{-1} to 64 m s^{-1} (16 m s^{-1} reduction) and 40 m s^{-1} to 32 m s^{-1} (8 m s^{-1} reduction, which is half the reduction at 80 m s^{-1}). Actually, the turbulence length scale in an axisymmetric model may affect the relationship between C_k/C_d and Vmax (Bryan and Rotunno, 2009; Bryan, 2012), but this does not imply that the turbulence length scale is a function of wind speed. There may also be concerns about going from the axisymmetric wavenumber (0 Vmax) to the Earth-relative wind anywhere in the storm. However, we believe that the problem of going from axisymmetric to point values would be small, given that we chose only storms that moved relatively slowly. Vukicevic et al. (2014) also showed that the azimuthal wavenumber 0+1 wind is strongly correlated with maximum intensity (as traditionally defined), which provides some additional support for our approximation.

Lastly, based on theory, the k in Equation 3.1 is the 10 m enthalpy at the radius of maximum winds (RMW), not the ambient enthalpy. However, it is technically challenging to calculate an accurate enthalpy at the RMW because the spatial resolution (1.5° × 1.5°) of the MERRA data used in the present analysis is not enough to resolve the eyewall and the uncertainty in the estimated RMW. Therefore, in this study, the enthalpy and MPI were calculated by averaging values within a 300 km radius of the storm center rather than using point values at the RMW. We also estimated the MPI using prestorm conditions (3 days before LMI) (Lin et al., 2013) to avoid modifications in the atmospheric and oceanic profiles due to air and moisture supply and oceanic mixing accompanied by TCs. A series of sensitivity experiments revealed that the averaging areas (100 km to 500 km or a donut-shaped path along the RMW) and the MPI calculation time (0 to 3 days before MPI) do not significantly affect the main results.

There are reasonably convincing studies for decreasing C_d and increasing C_k under severe wind. As wind speed increases, the ocean becomes covered by foam

and C_d is reduced due to the slippery surface after the foam at the air-sea interface disappeared (Powell et al., 2003). Donelan (2018) showed that C_d decreased due to the sheltering of the surface in the lee of steep waves. Soloviev et al. (2014) suggest that C_d can also decrease because the KH instability at the air-sea interface leads to an absence of short surface waves (the instability grows more quickly due to large shear for short waves). It is known that sea spray is a crucial factor in the development of TCs, which are responsible for the enhancement of energy flux from the ocean to the atmosphere (Andreas and Emanuel, 2001, Andreas, 2011). Andreas (2011) projected a significant C_k increase with wind speed because of the increasing importance of spray-mediated transfer although the C_k ratio is varied with surface temperature and atmosphere stratification.

An accurate estimation of air-sea enthalpy and momentum fluxes is key to improving intensity forecast accuracy in numerical weather prediction models (Sroka and Emanuel, 2021). Whether C_k/C_d decreases or increases at extreme winds above 50 m s^{-1} remains debatable. Limitations also exist in our method of estimating C_k/C_d. Nevertheless, this study provides important clues for understanding C_k/C_d behavior at high winds, where field observations are difficult. We also show through real TCs simulations that applying the new C_k/C_d parameterization to TC prediction can significantly reduce the negative intensity bias. However, numerical experiments and verifications in more cases are needed to generalize the present results. Our prediction results still show negative biases in high winds, suggesting that other factors, such as sea spray and TC model physics should be further improved.

4. Conclusion

Efforts have been directed toward improving for the TC intensity prediction, however, enhancing the prediction skills for a rapid intensification and extremely intense TC is still a big challenge for researchers. This study has been conducted to improve TC intensity predictions of statistical-dynamical model and dynamical model using two methods, advanced predictors and novel air-sea exchange coefficients on the bases of Emanuel's MPI.

To improve statistical prediction methods, we suggested the *NGR* index, which was calculated by using *DAT* and wind dependent C_d instead of SST and constant C_d, respectively. The NGR_{50}-w which is wind speed dependent *NGR* based on temperature averaged over top 50 m, showed the highest correlation (r=0.69) with 24-h TC intensity change, compared with *DAT*-based intensification potential (POT_{50}, r=0.48) and *NGR* with constant C_d based on temperature averaged over top 90 m (NGR_{90}-t, r=0.64). To demonstrate the effectiveness of NGR_{50}-w, a perfect prognosis-based multiple linear regression models have been developed for 24-h intensity change over the WNP based on a combination of NGR_{50}-w and commonly used important predictors in statistical models, *PER*, *SHRD*, and conducted experiments for training (2004-2014) and test (2015-2016) periods. With the same PER and SHRD predictors, the statistical model with the NGR_{50}-w improves upon the model with POT_{50} or NGR_{90}-t by about 16%.

A new parameterization of the ratio of C_k/C_d under major tropical cyclones above 40 m s^{-1} has been estimated by matching observed LMI of TCs with the theoretical *MPI* under idealized conditions. The ratio of C_k/C_d has been estimated using both *SST* and *DAT* (from the surface to a depth of 80 m) based *MPI* have been calculated, resulting in increases with wind speed at extreme winds above 40 m s^{-1}. These findings are qualitatively consistent with previous research. The increasing C_k/C_d ratio can mean that C_d decreases, or C_k increases, or both C_d decreases and C_k

increases. There are convincing studies for decreasing C_d and increasing C_k. Powell et al. (2003) estimated C_d in a TC using in situ data collected from GPS dropsonde, resulting in C_d decrease with wind speed above 40 m s^{-1}. They showed that the ocean becomes completely covered by foam as wind speed increases and C_d is reduced due to increased foam coverage at the air-sea interface. Holthuijsen et al. (2012) also analyzed many more profiles from GPS sonde data to estimate C_d and their experiment results were consistent with those in Powell et al. (2003). Kudryavtsev and Makin (2011) showed that sea spray could significantly influence the C_d using marine near-surface air boundary layer in very high wind speeds. They found that the suspended sea spray influences the atmospheric boundary layer turning into saturation with the spume droplets, resulting in decrease of the C_d. Andreas (2011) esimtated a significant C_k increase with wind speed because of the increasing importance of spray-mediated transfer. This estimate of C_k increases sharply in agreement with some more recently published coefficients from Troitskaya et al. (2018) used empirical models and Komori et al. (2018) used laboratory measurement. The impact of the new parameterization of C_k/C_d has been examined using HWRF model for idealized experiments and real-case predictions. To examine the individual impact of the coefficients on TC intensity, two types of increasing C_k/C_d parameterization were employed, Cd_DC and Ck_IC, and these were compared with CTRL. The idealized experiments demonstrated that both decreasing C_d and increasing C_k at extreme winds positively provide favorable conditions for TC intensification, but decreasing C_d is more significant than increasing C_k because C_d affects reducing sea surface cooling as well as increasing heat fluxes. As a result, for the real TC cases, bias and errors of Cd_DC are significantly reduced at most forecast lead times while Ck_IC forecasts are not significantly improved compared to CTRL.

These new *NGR* index and parameterization of C_k/C_d should help to improve maximum potential intensity theory and our understanding of TC intensity change and intensification. It is expected that the *NGR* as a new predictor, which has a higher correlation with TC intensity, will contribute to improvement in prediction skills for a

statistical-dynamical model. From a dynamic modeling perspective, the estimation of C_k/C_d provides additional confidence in an improved surface layer schemes that increase air-sea exchange coefficients as the wind speeds increase above 40 m s^{-1}, which significantly improves the underestimation of strong TC intensity.

Several additional studies that deserve further attention. Instead of using the *DAT* and soloviev et al (2014)'s C_d, TC-induced mixing depth varying with an individual TC state and new parameterization of C_d will be examined. In addition, advanced *NGR* will be investigated considering normalized TC intensity to better include RI prediction. The *NGR* index could be applied to other years and TC basins, Atlantic, eastern North Pacific, etc. At the same time, to improve statistical dynamical model skills, machine learning techniques for better TC intensity prediction could be considered as an alternative to multi-linear regression. Also, the effectiveness of Cd_DC will be demonstrated using coupled ocean atmosphere wave sediment transport system to understand the wave-current interaction process. In addition, the effectiveness and generization of the new parameterizaion of C_k/C_d should be made with more numerical experiments.

Appendix

The new formulation for z_o a used in the Cd_DC experiment is

$$Z_0 = \exp(p10 + p11 \times W + p12 \times W^2 + p13 \times W^3),\ W \leq 6.5\, m\, s^{-1}$$

$$Z_0 = p25 \times W^5 + p24 \times W^4 + p23 \times W^3 + p22 \times W^2 + p21 \times W + p20,\ 6.5\, m\, s^{-1} < W \leq 15.7\, m\, s^{-1}$$

$$Z_0 = \exp(p35 \times W^5 + p34 \times W^4 + p33 \times W^3 + p32 \times W^2 + p31 \times W + p30,\ 15.7\, m\, s^{-1} < W \leq 46.0\, m\, s^{-1}$$

$$Z_0 = 10 \times \left(\frac{1}{\exp\sqrt{\frac{0.16}{p45 \times W^5 + p44 \times W^4 + p43 \times W^3 + p42 \times W^2 + p41 \times W + p40}}}\right),\ W > 46.0\, m\, s^{-1}$$

where W (m s^{-1}) is the wind speed,

p10 = -8.396975715683501e+00, p11 = -1.597898515251717e+00,

p12 = 2.855780863283819e-01, p13 = -1.296521881682694e-02,

p20 = 2.147264020369413e-05, p21 = 1.739759082358234e-07,

p22 = -1.240239171056262e-06, p23 = 1.962282433562894e-07,

p24 = 3.281964357650687e-09, p25 = 3.790846746036765e-10,

p30 = -1.663993561652530e+01, p31 = 1.255457892775006e+00,

p32 = -6.139315534216305e-02, p33 = 1.735308193700643e-03,

p34 = -2.793849676757154e-05, p35 = 1.840430200185075e-07,

p40= -0.016943180834872e+00, p41= 0.001980799375510e+00,

p42= -7.499441958611604e-05, p43= 1.330088992305179e-06,

p44= -1.138431432537254e-08, p45= 3.806734376022113e-11

References

Andreas, E. L. and Emanuel, K. A. (2001). Effects of sea spray on tropical cyclone intensity. *Journal of the atmospheric sciences*, **58(24)**, 3741-3751.

Andreas, E. L. (2011). Fallacies of the enthalpy transfer coefficient over the ocean in high winds. *Journal of the Atmospheric Sciences,* **68**, 1435-1445.

Balaguru, K., Foltz, G. R., Leung, L. R., D'Asaro, E., Emanuel, K. A., Liu, H., and Zedler, S. E. (2015). Dynamic potential intensity: An improved representation of the ocean's impact on tropical cyclones. *Geophys. Res. Lett.* **42**, 6739–6746.

Balaguru, K., Foltz, G. R., Leung, L. R., Hagos, S. M., and Judi, D. R. (2018). On the use of ocean dynamic temperature for hurricane intensity forecasting. *Wea. Forecasting,* **33***,* 411–418.

Bao, J.-W., Fairall, C. W., Michelson, S. A. and Bianco, L. (2011). Parameterization of sea-spray impact on the air-sea momentum and heat fluxes. *Monthly Weather Review*, **139**, 3781-3797.

Bao, J.-W., Gopalakrishnan, S. G., Michelson, S. A., Marks, F. D., and Montgomery, M. T. (2012). Impact of physics representations in the HWRFX model on simulated hurricane structure and wind–pressure relationships. *Mon. Wea. Rev.,* **140**, 3278–3299.

Bell, M. M., Montgomery, M. T., and Emanuel, K. A. (2012). Air-sea enthalpy and momentum exchange at major hurricane wind speeds observed during CBLAST. *J. Atmos. Sci*. **69**, 3197–3222.

Bister, M., and Emanuel, K. A. (1998). Dissipative heating and hurricane intensity. *Meteor. Atm. Phys*., **52**, 233–240.

Biswas, M. K., Abarca, S., Bernardet, L., Ginis, I., Grell, E., Iacono, M., et al. (2018). Hurricane Weather Research and Forecasting (HWRF) Model: 2017 Scientific Documentation (Technical Report). Boulder, CO: National Center for Atmospheric Research and Developmental Testbed Center.

Black, P. G., D'Asaro, E. A., Sanford, T. B., Drennan, W. M., Zhang, J. A., French, J. R., et al. (2007). Air-sea exchange in hurricanes: Synthesis of observations from the Coupled Boundary Layer Air-Sea Transfer Experiment. *Bulletin of the American Meteorological Society*, 88, 357-374.

Braun, S. A. and Tao, W.-K. (2000). Sensitivity of high-resolution simulations of Hurricane Bob (1991) to planetary boundary layer parameterizations. *Mon. Wea. Rev*., **128**, 3941–3961.

Bryan, B. H. and Rotunno, R. (2009). The Maximum Intensity of Tropical Cyclones in Axisymmetric Numerical Model Simulations. *Monthly Weather Review*, **137**, 1770-1789.

Bryan, B. H. (2012). Effects of surface exchange coefficients and turbulence length scales on the intensity and structure of numerically simulated hurricanes. *Monthly Weather Review,* **140**, 1125-1143.

Chen, H. and Gopalakrishnan, S. (2014). A study on the asymmetric rapid intensification of Hurricane Earl (2010) using the HWRF system. *Proc. 31st Conference on Hurricanes and Tropical Meteorology*. San Diego, CA, 17D.5.

Chen, P., Yu, H. and Chan, J. C. L. (2011). A western North Pacific tropical cyclone intensity prediction scheme. *Acta Meteor. Sin.,* **25**, 611–624.

Chen, Y. and Yu, X. (2016). Enhancement of wind stress evaluation method under storm conditions. *Climate dynamics*, **47(12)**, 3833-3843.

Chen, Y., Zhang, F., Green, B. W. and Yu, X. (2018). Impacts of ocean cooling and reduced wind drag on Hurricane Katrina (2005) based on numerical simulations. *Monthly Weather Review*, **146(1)**, 287-306.

Chu, P.-S. and Zhao, X. (2007). A Bayesian regression approach for predicting tropical cyclone activity over the central North Pacific. *J. Climate,* **20**, 4002–4013.

Cloud, K. A., Reich, B. J., Rozoff, C. M., Alessandrini, S., Lewis, W. E. and Delle Monache, L. (2019). A feed forward neural network based on model output statistics for short-term hurricane intensity prediction. *Weather and Forecasting*,

34(4), 985-997.

Curcic, M. and Haus, B. K. (2020). Revised estimates of ocean surface drag in strong winds. *Geophysical Research Letters*, **47**, 32020GL087647.

DeCosmo, J., Katsaros, K. B., Smith, S. D., Anderson, R. J., Oost, W. A., Bumke, K., et al. (1996). Air-sea exchange of water vapor and sensible heat: The Humidity Exchange over the Sea (HEXOS) results. *Journal of Geophysical Research*, **101**, 12001-12016.

DeMaria, M. and Kaplan, J. (1994). A statistical hurricane intensity prediction scheme (SHIPS) for the Atlantic basin. *Wea. Forecasting,* **9**, 209–220.

DeMaria, M., and Kaplan, J. (1999). An updated statistical hurricane intensity prediction scheme (SHIPS) for the Atlantic and eastern North Pacific basins. *Wea. Forecasting*, **14**, 326–337.

DeMaria, M., Mainelli, M., Shay, L. K., Knaff, J. A. and Kaplan, J. (2005). Further improvements to the Statistical Hurricane Intensity Prediction Scheme (SHIPS). *Wea. Forecasting*, **20**, 531–543.

DeMaria, M., Knaff, J. A., and Kaplan, J. (2006). On the decay of tropical cyclone winds crossing narrow landmasses. *Journal of applied meteorology and climatology*, **45(3)**, 491-499.

DeMaria, M., DeMaria, R. T., Knaff, J. A. and Molenar, D. (2012). Tropical cyclone lightning and rapid intensity change. *Mon. Wea. Rev.,* **140**, 1828–1842.

DeMaria, M., Sampson, C. R., Knaff, J. A. and Musgrave, K. D. (2014). Is tropical cyclone intensity guidance improving?. *Bull. Amer. Meteorol. Soc.*, **95***,* 387–398.

Donelan, M. A., Haus, B. K., Reul, N., Plant, W. J., Stianssnie, M., Graber, H. C., Brown, O. B. and Saltzman, E. S. (2004). On the limiting aerodynamic roughness of the ocean in very strong winds. *Geophys. Res. Lett.,* **31***,* L18306.

Donelan, M. A. (2018). On the decrease of the oceanic drag coefficient in high winds. *Journal of Geophysical Research: Oceans*, **123(2)**, 1485-1501.

Elsberry, R. L., Chen, L., Davidson, J., Rogers, R., Wang, Y. and Wu, L. (2013). Advances in understanding and forecasting rapidly changing phenomena in

tropical cyclones. *Trop. Cyclone Res. Rev.* **2**, 13–24.

Emanuel, K. A. (1986). An air-sea interaction theory for tropical cyclones. Part I: Steady-state maintenance. *J. Atmos. Sci.* **43**, 585–604.

Emanuel, K. A. (1988). The maximum intensity of hurricanes. *J. Atmos. Sci.* **45**, 1143–1155.

Emanuel, K. A. (1995). Sensitivity of tropical cyclones to surface exchange coefficients and a revised steady-state model incorporating eye dynamics. *J. Atmos. Sci.* **52**, 3969–3976.

Emanuel, K. A. (2003). A similarity hypothesis for air–sea exchange at extreme wind speeds. *J. Atmos. Sci.* **60**, 1420–1428.

Emanuel, K. A., DesAutels, C., Holloway, C. and Korty, R. (2004). Environmental control of tropical cyclone intensity. *J. Atmos. Sci.,* **61**, 843–858.

Emanuel, K. A. and Rotunno, R, (2011). Self-stratification of tropical cyclone outflow. Part I: Implications for storm structure. *Journal of the Atmospheric Sciences*, **68**, 2236-2249.

Fan, Y., Ginis, I. and Hara, T. (2009). The effect of wind-wave-current interaction on air-sea momentum fluxes and ocean response in tropical cyclones. *J. Phys. Oceanogr.* **39**, 1019–1034.

Fan, Y., Ginis, I. and Hara, T. (2010). Momentum flux budget across the air-sea interface under uniform and tropical cyclone winds. *J. Phys. Oceanogr.* **40**, 2221–2242.

French, J. R., Drennan, W. M., Zhang, J. A. and Black, P. G. (2007). Turbulent fluxes in the hurricane boundary layer. Part I: Momentum flux. *Journal of the Atmospheric Sciences*, **64**, 1089-1102.

Gall, R., Franklin, J., Marks, F., Rappaport, E. N. and Toepfer, F. (2013). The Hurricane Forecast Improvement Project. *Bull. Amer. Meteor. Soc.* **94**, 329–343.

Gao, S., Zhang, W., Liu, J., Lin, I.-I., Chiu, L. S. and Cao, K. (2016). Improvements in typhoon intensity change classification by incorporating an ocean coupling potential intensity index into decision trees. *Wea. Forecasting,*

31, 95–106.

Goni, G., DeMaria, M., Knaff, J., Sampson, C., Ginis, I., Bringas, F., Mavume, A. , Lauer, C., Lin, I.-I., Sandery, P., Ramos-Buarque, S., Kang, K., Mehra, A., Chassignet, E. P. and Halliwell, G. (2009). Applications of satellite-derived ocean measurements to tropical cyclone intensity forecasting. *Oceanography*, **22(3)**, 190–197.

Gray, W., Ruprecht, E. and Phelps, R. (1975). Relative humidity in tropical weather systems. *Monthly Weather Review*, **103**, 685–690.

Green, B. W. and Zhang, E. (2013). Impacts of air–sea flux parameterizations on the intensity and structure of tropical cyclones. *Mon. Weather Rev.* **141**, 2308–2324.

Haus, B. K., Jeong, D., Donelan, M. A., Zhang, J. A. and Savelyev, I. (2010). Relative rates of sea-air heat transfer and frictional drag in very high winds. *Geophysical Research Letters*, **37**, L07802.

Holland, G. J. (1997). The maximum potential intensity of tropical cyclones. *J. Atmos. Sci.* **54**, 2519–2541.

Holthuijsen, L. H., Powell, M. D. & Pietrzak, J. D. (2012): Wind and waves in extreme hurricanes. *J. Geophys. Res.* **117**, C09003.

Hsu, J. Y., Lien, R. C., D'Asaro, E. A. and Sanford, T. B. (2019). Scaling of drag coefficients under five tropical cyclones. *Geophysical Research Letters*, **46**, 3349-3358.

Jarosz, E., Mitchell, D. A., Wang, D. W. and Teague, W. J. (2007). Bottom-up determination of air-sea momentum exchange under a major tropical cyclone. *Science,* **315**, 1707–1709.

Jeong, D., Haus, B. K. and Donelan, M. A. (2012). Enthalpy transfer across the air–water interface in high winds including spray. *Journal of the atmospheric sciences*, **69(9)**, 2733-2748.

Jenkins, A. D. (2002). Do strong winds blow waves flat?. *In Ocean Wave Measurement and Analysis (2001)* (pp. 494-500).

Kaplan, J. and DeMaria, M. (2003). Large-scale characteristics of rapidly intensifying

tropical cyclones in the North Atlantic basin. *Weather and forecasting*, **18(6)**, 1093-1108.

Kaplan, J., DeMaria, M. and Knaff, J. A. (2010). A revised tropical cyclone rapid intensification index for the Atlantic and eastern North Pacific basins. *Wea. Forecasting,* **25**, 220–241.

Kaplan, J. and Coauthors (2015). Evaluating environmental impacts on tropical cyclone rapid intensification predictability utilizing statistical models. *Wea. Forecasting*, **30**, 1374-1396.

Kudryavtsev, V. N. & Makin, V. K. (2011): Impact of ocean spray on the dynamics of the marine atmospheric boundary layer. *Boundary-Laer Meteorol.* **140**, 383-410.

Kim, S.-H., Moon, I.-J. and Chu, P.-S. (2018). Statistical-dynamic typhoon intensity predictions in the western North Pacific using track pattern clustering and ocean coupling predictors. *Wea. Forecasting,* **33**, 347–365.

Knaff, J. A., Sampson, C. R. and DeMaria, M. (2005). An operational Statistical Typhoon Intensity Prediction Scheme for the western North Pacific. *Wea. Forecasting*, **20**, 688–699.

Knaff, J. A., Sampson, C. R. and Musgrave, K. D. (2018). An operational rapid intensification prediction aid for the western North Pacific. *Weather and Forecasting*, **33(3)**, 799-811.

Knapp, K. R., Kruk, M. C., Levinson, D. H., Diamond, H. J. and Neumann, C. J. (2010). The International Best Track Archive for Climate Stewardship (IBTrACS): Unifying tropical cyclone data. *Bulletin of the American Meteorological Society*, **91**, 363-376.

Knutson, T., Camargo, S. J., Chan, J. C., Emanuel, K., Ho, C. H., Kossin, J., & Coauthors. (2020). Tropical cyclones and climate change assessment: Part II: Projected response to anthropogenic warming. *Bulletin of the American Meteorological Society*, **101(3)**, E303-E322.

Komori, S., Iwano, K., Takagaki, N., Onishi, R., Kurose, R., Takahashi, K. &

Suzuki, N. (2018). Laboratory measurements of heat transfer and drag coefficients at extremely high wind speeds. *J. Phys. Oceanography*, **48**, 959-974.

Li, F. N., Song, J. B., He, H. L., Li, S., Li, X. and Guan, S. D. (2016). Assessment of surface drag coefficient parametrizations based on observations and simulations using the Weather Research and Forecasting model. *Atmospheric and Oceanic Science Letters*, **9**, 327-336.

Lin, I.-I., Wu, C. C., Pun, I. F. and Ko, D. S. (2008). Upper-ocean thermal structure and the western North Pacific category-5 typhoons. Part I: Ocean features and category-5 typhoon's intensification. *Mon. Wea. Rev.* **136**, 3288–3306.

Lin, I.-I., Chen, C.-H., Pun, I.-F., Liu, W. T. and Wu, C.-C. (2009). Warm ocean anomaly, air sea fluxes, and the rapid intensification of tropical cyclone Nargis (2008). *Geophys. Res. Lett.* **36**, *L03817.*

Lin, I.-I., and coauthors (2013). An ocean coupling potential intensity index for tropical cyclones. *Geophys. Res. Lett*. **40**, 1878–1882.

Lin, N., Jing, R., Wang, Y., Yonekura, E., Fan, J. and Xue, L. (2017). A statistical investigation of the dependence of tropical cyclone intensity change on the surrounding environment. *Mon. Wea. Rev.* **145**, 2813–2831.

Liu, L., Wang, G., Zhang, Z. and Wang, H. (2022). Effects of Drag Coefficients on Surface Heat Flux during Typhoon Kalmaegi (2014). Advances in Atmospheric Sciences, **39(9)**, 1501–1518.

Mei, W. and Xie, S.-P. (2016). Intensification of landfalling typhoons over the northwest Pacific since the late 1970s. *Nature. Geoscience.,* **9**, 753–757.

Montgomery, M. T., Smith, R. K. and Nguyen, S. V. (2010). Sensitivity of tropical-cyclone models to the surface drag coefficient. *Q. J. R. Meteorol. Soc.* **136**, 1945–1953.

Moon, I.-J., Ginis, I. and Hara, T. (2004). Effect of surface waves on air-sea momentum exchange. Part II: Behavior of drag coefficient under tropical cyclone. *Journal of the Atmospheric Sciences*, **61**, 2344-2348.

Moon, I.-J., Ginis, I., Hara, T. and Thomas, B. (2007). A physics-based

parameterization of air–sea momentum flux at high wind speeds and its impact on hurricane intensity predictions. *Mon. Wea. Rev.* **135**, 2869–2878.

Mueller, J. A. and Veron, F. (2014). Impact of sea spray on air-sea fluxes. Part II: Feedback effects. *Journal of Physical Oceanography*, **44**, 2835–2853.

Murakami, H., Wang, B., Li, T. and Kitoh, A. (2013). Projected increase in tropical cyclones near Hawaii. *Nat. Clim. Change*, **3**, 749-754.

Nolan, D. S., Zhang, J. A. and Stern, D. P. (2009a). Evaluation of planetary boundary layer parameterizations in tropical cyclones by comparison of in situ observations and high-resolution simulations of Hurricane Isabel (2003). Part I: Initialization, maximum winds, and the outer-core boundary layer. *Mon. Wea. Rev.* **137**, 3651–3674.

Nolan, D. S., Stern, D. P. and Zhang, J. A. (2009b). Evaluation of planetary boundary layer parameterizations in tropical cyclones by comparison of in situ observations and high-resolution simulations of Hurricane Isabel (2003). Part II: Inner-core boundary layer and eyewall structure. *Mon. Wea. Rev.* **137**, 3675–3698.

Ooyama, K. (1969). Numerical simulation of the life cycle of tropical cyclones. *J. Atmos. Sci.* **26**, 3-40.

Powell, M. D., Vickery, P. J. and Reinhold, T. A. (2003). Reduced drag coefficient for high wind speeds in tropical cyclones. *Nature,* **422**, 279–283.

Price, J. F., Sandford, T. B. and Forristall, G. Z. (1994). Forced stage response to a moving hurricane. *Journal of Physical Oceanography*, **24**, 233-260.

Price, J. F. (2009). Metrics of hurricane-ocean interaction: Vertically-integrated or vertically-averaged ocean temperature?. *Ocean Sci.* **5**, 351–368.

Pun, I. F., Lin, I.-I., Wu, C. R., Ko, D. S. and Liu, W. T. (2007). Validation and application of altimetry-derived upper ocean thermal structure in the Western North Pacific Ocean for typhoon intensity forecast. *IEEE Trans. Geosci. Remote Sens.* **45(6)**, 1616–1630.

Quenouille, M. A. (1952). Associated mesurements. *Associated Measurements*,

Butterworths, 242 pp.

Rappaport, E. N., Jiing, J. G., Landsea, C. W., Murillo, S. T. and Franklin, J. L. (2012). The joint hurricane testbed—Its first decade of tropical cyclone research-to-operations activities revisited. *Bull. Am. Meteor. Soc.* **93**, 371–380.

Richter, D. H. and Stern, D. P. (2014). Evidence of spray-mediated air-sea enthalpy flux within tropical cyclones. *Geophysical Research Letters*, **41**, 2997-3003.

Richter, D. H., Bohac, R. and Stern, D. (2016). An assessment of the flux profile method for determining air-sea momentum and enthalpy fluxes from dropsonde data in tropical cyclones. *Journal of the Atmospheric Sciences*, **73**, 2665-2682.

Richter, D. H., Wainwright, C., Stern, D. P., Bryan, G. H. and Chavas, D. (2021). Potential low bias in high-wind drag coefficient inferred from dropsonde data in hurricanes. *Journal of the Atmospheric Sciences*, **78(7)**, 2339-2352.

Rosenthal, S. L. (1971). The response of a tropical cyclone model to variations in boundary layer parameters, initial conditions, lateral boundary conditions, and domain size. *Monthly Weather Review*, **99**, 767-777.

Rotunno, R. and Emanuel, K. A. (1987). An air-sea interaction theory for tropical cyclones. Part II: Evolutionary study using a nonhydrostatic axisymmetric numerical model. *J. Atmos. Sci.* **44**, 542–561.

Rozoff, C. M. and Kossin, J. P. (2011). New probabilistic forecast models for the prediction of tropical cyclone rapid intensification. *Wea. Forecasting,* **26**, 677–689.

Shay, L. K., Goni, G. J. and Black, P. G. (2000). Effects of a warm oceanic feature on Hurricane Opal. *Mon. Wea. Rev.* **128**, 1366–1383.

Soloviev, A. V., Lukas, R., Donelan, M. A., Haus, B. K. and Ginis, I. (2014). The air-sea interface and surface stress under tropical cyclones. *Sci. Rep.* **4**, 5306.

Soloviev, A. V., Lukas, R., Donelan, M. A., Haus, B. K. and Ginis, I. (2017). Is the state of the air-sea interface a factor in rapid intensification and rapid decline of tropical cyclones?. *J. Geophys. Res., Oceans.* **122**.

Sroka, S. and Emanuel, K. A. (2021). A review of parameterizations for enthalpy

and momentum fluxes from sea spray in tropical cyclones. *Journal of Physical Oceanography*, **51**, 3053-3069.

Takagaki, N., Komori, S., Suzuki, N., Iwano, K., Kuramoto, T., Shimada, S., Kurose, R. and Takahashi, K. (2012). Strong correlation between the drag coefficient and the shape of the wind sea spectrum over a broad range of wind speeds. *Geophys. Res. Lett.* **39***, L23604,* doi.: 10.1029/2012GL053988.

Tallarpragada, V. and Kieu, C. (2014). Real-time forecasts of typhoon rapid intensification in the north Western Pacific basin with the NCEP operational HWRF model. *Trop. Cyclone Res. Rev.* **3(2)***,* 63–76.

Troitskaya, Y., Druzhinin, O., Kozlov, D. & Zilitinkevich, S. (2018). The "bag breakup" spume droplet generation mechanism at high winds. Part II: Contribution to momentum and enthalpy transfer. *J. Phys. Oceanogr.* **48**, 2189-2297.

Vickery, P. J., Wadhera, D., Powell, M. D. and Chen, Y. (2009). A hurricane boundary layer and wind field model for use in engineering applications. *Journal of Applied Meteorology Climatology*, **48**, 381-405.

Vukicevic, T., Uhlhorn, E. and Reasor, P. (2014). A Novel multiscale intensity metric for evaluation of tropical cyclone intensity forecasts. *Journal of the Atmospheric Sciences*, **71**, 1292-1304.

Wada, A. and Usui, N. (2007). Importance of tropical cyclone heat potential for tropical cyclone intensity and intensification in the Western North Pacific. *J. Oceanogr.* **63**, 427–447.

Wang, Y. and Wu, C. C. (2004). Current understanding of tropical cyclone structure and intensity changes-a review. *Meteorology and Atmospheric Physics.* **87**, 257-278.

Wilks, D. S. (2011). *Statistical Methods in the Atmospheric Sciences*, 3rd ed., Elsevier, 676 pp.

Xu, W., Balaguru, K., August, A., Lalo, N., Hodas, N., DeMaria, M. and Judi, D. (2021). Deep learning experiments for tropical cyclone intensity forecasts.

Weather and Forecasting, **36(4)**, 1453-1470.

Yoshida K., Sugi, M., Mizuta, R., Murakami, H. and Ishii, M. (2017). Future changes in tropical cyclone activity in high-resolution large-ensemble simulations. *Geophys. Res. Lett*. **44**, 9910-9917, doi: 10.1002/2017GL075058.

Zhang, J. A., Black, P. G., French, J. R. and Drennan, W. M. (2008). First direct measurements of enthalpy flux in the hurricane boundary layer: The CBLAST results. *Geophysical Research Letters*, **35**, L14813.

Zhang, F. and Tao, D. (2013). Effects of vertical wind shear on the predictability of tropical cyclones. *J. Atmos. Sci.* **70**, 975–983.